ARTICLE IN PRESS

Available online at www.sciencedirect.com

ScienceDirect

Atmospheric Environment ▮ (▮▮▮▮) ▮▮▮–▮▮▮

ATMOSPHERIC ENVIRONMENT

www.elsevier.com/locate/atmosenv

Aerosol optical properties and related chemical apportionment at Xinken in Pearl River Delta of China

Y.F. Cheng[a], A. Wiedensohler[b], H. Eichler[b,1], H. Su[a], T. Gnauk[b], E. Brüggemann[b], H. Herrmann[b], J. Heintzenberg[b], J. Slanina[a], T. Tuch[b], M. Hu[a], Y.H. Zhang[a,*]

[a]*College of Environmental Sciences and Engineering, Peking University, 100871 Beijing, China*
[b]*Leibniz-Institute for Tropospheric Research, 04318 Leipzig, Germany*

Received 17 September 2007; received in revised form 13 February 2008; accepted 19 February 2008

Abstract

Aerosol optical properties (AOPs) of sub-10 μm particles under dry conditions (relative humidity (RH) <20%) were investigated at Xinken in Pearl River Delta of China from 4 October to 5 November 2004. Severe aerosol optical pollution has been found characterized by strongly light-absorbing particles. At 550 nm, the magnitude of the light scattering ($333 \pm 138\,Mm^{-1}$) and absorption ($70 \pm 42\,Mm^{-1}$), limited visual range (5.3 ± 2.5 km), and low single scattering albedo (0.83 ± 0.05) show Xinken to be comparable to the most polluted urban cores rather than even a polluted rural site. Other presented AOPs include hemispheric backscattering fraction ($11 \pm 1\%$) and asymmetry parameter (0.67 ± 0.01) at 550 nm, and Ångström exponent ($\mathring{a}_{450/700} = 1.6 \pm 0.15$). Systematic relationships exist among the various AOPs. Their diurnal variations cannot be solely explained with the development of atmospheric boundary layer, but also obviously influenced by local wind patterns, variation of sources, photochemistry and nighttime heterogeneous chemistry. The fractional contributions to extinction, scattering and absorption ($f_{ep;sp;ap}$) due to sub-aerosol-populations and individual chemical compounds are derived by the Mie simulations. The sub-1 μm particles contribute more than 90% of the particle extinction ($\sigma_{ep,550\,nm}$). Under dry conditions, f_{ep} of non-sea-salt sulfate, particulate organic matter, elemental carbon (EC) and residual are about 44%, 17%, 17% and 15%, respectively. However, the water uptake of particles can contribute 50–60% to $\sigma_{ep,550\,nm}$ at RH 90%. So in the ambient atmosphere, sulfate, carbonaceous material and water all play very important roles, concerning the visibility impairment at Xinken. The respective mass extinction, scattering and absorption efficiencies ($\alpha_{ep;sp;ap}$) are mostly consistent with previously reported values for the polluted area. $\alpha_{ap,EC,550\,nm}$ for sub-1 μm and sub-10 μm ranges are 9.3 ± 1.4 and $7.2 \pm 1.0\,m^2\,g^{-1}$, respectively. Our results imply a higher $\alpha_{ap,EC}$ for more internally mixed EC under the atmospheric conditions present at Xinken.

Keywords: Aerosol optical properties; Chemical apportionment; Mass extinction/scattering efficiency; Specific attenuation cross-section; PRD of China

*Corresponding author. Tel.: +86 10 62756592; fax: +86 10 62751927.
E-mail address: yhzhang@pku.edu.cn (Y.H. Zhang).
[1]Now at: Institute for Atmospheric Physics, Johannes Gutenberg-University, Mainz D-55099, Germany.

1352-2310/$ - see front matter © 2008 Elsevier Ltd. All rights reserved.
doi:10.1016/j.atmosenv.2008.02.034

1. Introduction

The scattering and absorption of solar radiation lead to the direct aerosol radiative forcing (IPCC, 2007), of which the magnitude and sign are depending on the particle chemical and microphysical properties, as well as the albedo of the underlying surface (Seinfeld and Pandis, 1998). In light of Chýlek and Wong (1995), several key aerosol optical properties (AOPs), including the atmospheric aerosol burden, single scattering albedo, upscatter fraction and the mass scattering and absorption efficiencies must be measured or estimated in order to evaluate the local or regional aerosol direct radiative forcing. These key parameters are directly related to the aerosol total light scattering, hemispheric backscattering and absorption properties. In the meantime, the amount of water taken up by the water soluble particle matters changes the particle size distributions and their refractive index ($\tilde{m}$) during the humidification, and hence also plays an important role in both visibility impairment and aerosol radiative forcing (Covert et al., 1972; Charlson et al., 1992).

Indeed, aerosols are one of the greatest sources of uncertainty in the assessment of global climate forcing (IPCC, 2007). This is mainly due to the complex connection between the radiative effects of tropospheric aerosol particles and their physical and chemical properties, and also their non-uniform spatial and temporal distributions (Seinfeld and Pandis, 1998; Quinn and Coffmann, 1998; Bond et al., 1998; Sheridan et al., 2001). However, detailed observations of the AOPs in China are still limited (Huebert et al., 2003). Therefore, widespread investigations, in particular of radiation-related aerosol properties, including aerosol light scattering and absorption characteristics, and size-segregated number and mass size distributions, as well as the relative humidity (RH) dependence of those properties, are essentially needed for a realistic estimations of the climatic and visibility impacts of present and future aerosol pollution in the quickly developing Pearl River Delta (PRD) area in Southeastern China.

In this paper, we present the one month record of in situ ground based aerosol optical measurements at Xinken in PRD during a polluted season from 4 October to 5 November 2004. Based on the size-segregated aerosol number and chemical characteristics, an optical related chemical apportionment has been accomplished with a Mie model in the external mixture. It is to find out the contributions of light extinction, scattering and absorption by sub-aerosol-populations and also individual chemical components. The contributions by water taken up are also discussed. Consequently, the mass extinction, scattering and absorption efficiencies are estimated.

2. Observations

As part of the Program of Regional Integrated Experiments of Air Quality over PRD 2004 (PRIDE-PRD2004), measurements of aerosol optical, chemical and physical properties, as well as the gas phase observations, were conducted from 4 October to 5 November 2004 (278–310 day of year (DOY)) at Xinken (22.6°N, 113.6° E). The Xinken site is located near the mouth of Pearl River and situated on the northwest–southeast axis between Guangzhou and Hong Kong. It is considered as a non-urban though regionally polluted site. However, the air pollution at Xinken is also influenced by some local sources, such as biomass burning, cooking, exhaust plums from diesel ships and so on.

Ground based measurements were mainly conducted inside an air-conditioned container (~22 °C). The sampling air was collected with a PM_{10} impactor inlet (16.67 L min^{-1}). A main adsorption drier (BOGE, Model DAZ6, RH < 10%) was used to supply the dry compressor air for the whole system. For particle number size distribution measurements, driers (RH < 10%, Birmili et al., 2004) based on Nafion membrane technology (Perma Pure LLC Inc., Toms River, NJ, USA) were installed. A set of silica-gel diffusion driers (RH < 20%, Wex, 2002) was placed upstream the aerosol optical measurements. Keeping the RH deliberately at the defined low value was mainly based on three reasons. The first is to measure the aerosol microphysical and optical properties which are intrinsic to the aerosol rather than dependent on atmospheric RH (Bergin et al., 1997; Carrico et al., 2003) and to ensure comparability between different aerosol measurements (Anderson and Ogren, 1998). Second, the obviously differences in temperature (T) between outside and indoors may change the T and RH of the aerosol flow. At last, some of the measurements cannot be carried out at high RHs. For example, the Humidified Differential Mobility Particle Sizer (IfT, Leipzig, Germany) (Eichler et al., 2008) needs to operate under the environment with

Please cite this article as: Cheng, Y.F., et al., Aerosol optical properties and related chemical apportionment at Xinken in Pearl River Delta of China. Atmospheric Environment (2008), doi:10.1016/j.atmosenv.2008.02.034

critically stable RH. An overview of the entire instrumentation can be found in Cheng et al. (2006).

2.1. Meteorological parameters

The meteorological parameters, wind speed (WS) and direction (WD), RH and T, were continuously measured at the Panyu meteorology station, roughly 1 km away from Xinken. The measurements represent hourly data sets of the above quantities in this paper.

The weather conditions during the whole campaign were typically clear to partly cloudy and no precipitation occurred. Fig. 1 depicts the meteorological conditions. The ambient T and RH showed a pronounced diurnal variation (Fig. 2a) with averages of $23.2 \pm 2.7\,^{\circ}C$ and $65 \pm 18\%$, respectively. The wind patterns can be classified into north/northeasterly (N/NE), south/southeasterly (S/SE, mainly started at ~20 : 00) and calm wind (CL, $\sim 0\,m\,s^{-1}$), with respective frequencies of 38%, 14% and 48%. The average WS of N/NE and S/SE winds were 2.7 ± 1.6 and $1.5 \pm 1.3\,m\,s^{-1}$, respectively. The RH in the nighttime during N/NE wind was obviously lower than those in the S/SE or CL winds. At last, it is worth to notice that during N/NE wind Xinken is mainly influenced by the pollution transportation from the inner China continent, e.g. Guangzhou, etc. While to the S/SE, Xinken is bounded by the coast of the South China Sea. Hong Kong is at also the S/SE about 70 km away.

2.2. Aerosol optical properties

Aerosol total scattering and hemispheric backscattering light coefficients (σ_{sp} and σ_{hbsp}) were measured with a high-sensitivity, three-wavelength, total/back scatter nephelometer at 450, 550 and 700 nm (TSI, Inc., Shoreview, MN USA, Model 3563) (Heintzenberg and Charlson, 1996; Anderson et al., 1996). Before and after the field campaign, calibrations were carried out with filtered particle-free air and CO_2 as the low and hight span gas. The differences between these two calibrations in the

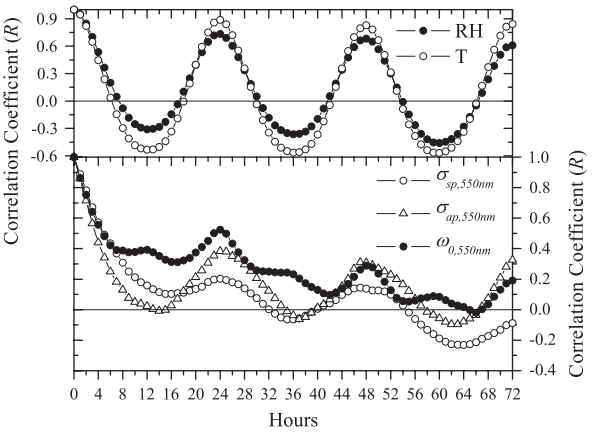

Fig. 2. Autocorrelation analysis of the meteorological parameters (ambient relative humidity (RH) and temperature (T)) and the optical properties at 550 nm (scattering and absorption coefficients ($\sigma_{sp;ap,550\,nm}$) and single scattering albedo ($\omega_{0,550\,nm}$)).

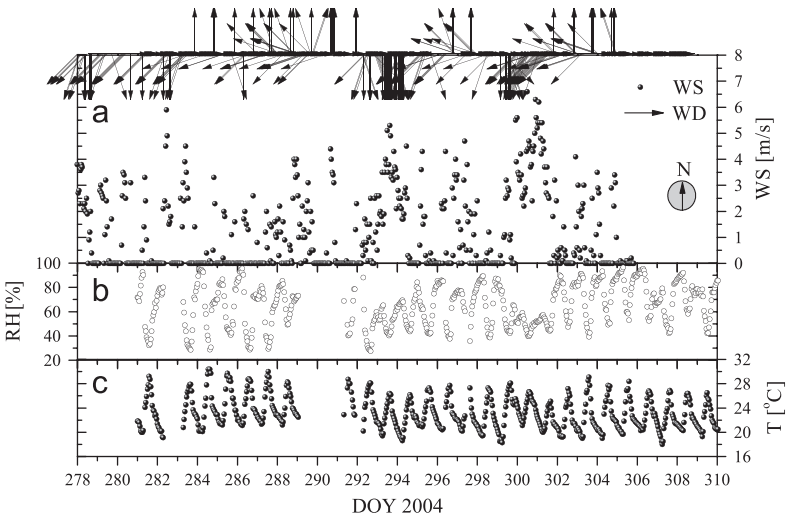

Fig. 1. Time series of the meteorological parameters during 278–310 DOY 2004 with a time resolution of 1 h. (a) presents the wind speed (WS) and direction (WD). (b) and (c) contain the ambient relative humidity (RH) and temperature (T), respectively.

Please cite this article as: Cheng, Y.F., et al., Aerosol optical properties and related chemical apportionment at Xinken in Pearl River Delta of China. Atmospheric Environment (2008), doi:10.1016/j.atmosenv.2008.02.034

slopes of the calibration lines for scatter and backscatter (K_2 and K_4), determined by measuring the normalized photo-counting rates associated with high and low span gases, were both within 3%. Zero baseline check was performed manually and periodically. Three hundred seconds was set as the averaging time. The data are averaged to 15 min. The uncertainty of TSI 3563 nephelometer at 99% confidence level has been estimated as 7% by Anderson et al. (1996).

However, the TSI 3563 integrating nephelometer measures and integrates the values of scattering intensity only over angles from 7° to 170° and from 90° to 170° to yield the $\sigma_{sp,neph}$ and $\sigma_{hbsp,neph}$, respectively. It means that the measured values are truncated in the near-forward and -backward angular ranges, compared with the realistic values. Furthermore, the light source is not exactly Lambertian, and shows a non-ideal angular response (Anderson et al., 1996) which is another systematic error of the measurement that must be corrected for. Based on the optical closure study at Xinken (Cheng et al., 2006), the angular truncation of the nephelometer data is corrected for total particle scattering coefficients at three wavelengths following the algorithm by Anderson and Ogren (1998) to yield the "measured" total scattering coefficient ($\sigma_{sp,e}$).

A Multi-angle Absorption Photometer (MAAP, Thermo, Inc., Waltham, MA USA, Model 5012) was used to measure the aerosol light absorption coefficient ($\sigma_{ap,MAAP}$). The instrument determines σ_{ap} from the simultaneous measurements of radiation passing through and scattered back from particles accumulating on a filter. It operates at three detection angles to resolve the influence of light-scattering aerosol components on the angular distribution of the back-scattered radiation (Petzold and Schönlinner, 2004). The flow rate of the MAAP was calibrated once per week and its variation was within 2%. This instrument yields the value as mass concentrations of black carbon in $\mu g\,m^{-3}$. According to the manual, an attenuation cross-section of $6.6\,m^2\,g^{-1}$ is used to convert the output data back to $\sigma_{ap,MAAP}$. The sampling frequency was 1 min and the data have been averaged to 15 min. The uncertainty of MAAP at 99% confidence level has been estimated as 12% by Petzold and Schönlinner (2004).

The wavelength of laser diode inside the MAAP was calibrated by a spectrometer. It has been found that the MAAP actually measures at the wavelength of 630 nm. Clarke et al. (2007) indicated that wavelength dependence of σ_{ap} is linked to particle size and composition. Their study revealed that absorption Ångström exponent changing from 0.7 to 1.1 for pollution aerosol and peaking near 1.3 for regional non-plume, while increasing to 2.1 for biomass burning plume. However, a conservative assumption of the inverse wavelength "Power Law" (Coen et al., 2004; Nessler et al., 2005) has been made here. Accordingly, the "measured" absorption coefficient at 550 nm ($\sigma_{ap,e,550\,nm}$) is calculated from $\sigma_{ap,MAAP,630\,nm}$ with $\sigma_{ap,550\,nm} = \sigma_{ap,630\,nm} \cdot (630/550)$.

An upper limit to the visibility (L_v, in units of km) can be estimated, using the dry aerosol optical measurements here and a modified Koschmieder relations with $L_v = 1.9/\sigma_{egp}$ (Griffing, 1980; Husar et al., 2000; Schichtel et al., 2001; Carrico et al., 2003). Here the extinction coefficient σ_{egp} is due to scattering and absorption by particles and gases in units of m^{-1}. The Koschmieder constant of 1.9 is about half of the standard value (3.92) (Seinfeld and Pandis, 1998). This factor of 2 reduction incorporates the fact that real visual targets are not black, they are frequently too small in angular size, and are located only at quantized distances away from the observer (Griffing, 1980).

Absorption of visible light by gases (σ_{ag}) is considered to be essentially due to NO_2 (Groblicki et al., 1981). Because it was not directly measured at Xinken, the average concentration of NO_2 has been roughly estimated as $\sim 36 \times 10^{-9}$ V/V with $[NO_2] = [NO_y] - [NO] - [HNO_3] - [HONO] - [Nitrate] - [Nitrite]$ (Su et al., 2008). NO_2 may be slightly overestimated here, since some other nitrogenous compounds are also counted as NO_y, e.g. peroxyacetyl nitrate. Based on the NO_2 concentration, $\sigma_{ag,550\,nm}$ can be estimated to be about $12\,Mm^{-1}$ with $\sigma_{ag} = 0.33 \cdot [NO_2]$ (Groblicki et al., 1981). Here, NO_2 are in units of $\times 10^{-9}$ V/V. In light of Fröhlich and Shaw (1980), Bucholtz (1995) and Tomasi et al. (2005), the Rayleigh scattering by gases ($\sigma_{sg,550\,nm}$) can be calculated as $11.3\,Mm^{-1}$ under the average surface T (296.4 K) and air pressure (1022 mbar) at Xinken.

The key intensive properties, independent of aerosol concentration, are derived from those extensive properties represented above. They are scattering Ångström exponent (Ångström, 1964) between 450 and 700 nm ($\mathring{a}_{450/700} = -\log(\sigma_{sp,450\,nm}/\sigma_{sp,700\,nm})/\log(450/700)$), hemispheric back scattering fraction ($\beta(1) = \sigma_{hbsp}/\sigma_{sp}$), and single scattering albedo ($\omega_0 = \sigma_{sp}/(\sigma_{sp} + \sigma_{ap})$).

Please cite this article as: Cheng, Y.F., et al., Aerosol optical properties and related chemical apportionment at Xinken in Pearl River Delta of China. Atmospheric Environment (2008), doi:10.1016/j.atmosenv.2008.02.034

2.3. Aerosol particle number size distribution

Under the dry conditions (RH < 10%), a Tandem Differential Mobility Particle Sizer (TDMPS, I*f*T, Leipzig, Germany) (Birmili et al., 1999) was used to measure the particle number size distributions with electrical mobility diameter from 3 to 900 nm. An Aerodynamic Particle Sizer (APS, TSI, Inc., Shoreview, MN USA, Model 3320) was operated to measure the particle number size distributions with aerodynamic diameters from 500 nm to 10 μm. The flow rates of the TDMPS and APS systems were calibrated once per week. The necessary quality checks, corrections and inversions of the data sets have been done (Cheng et al., 2006). The complete dry particle number size distributions (3 nm–10 μm) in Stokes diameter are result of combining TDMPS and APS data (Cheng et al., 2006) with the time resolution of 15 min. At 99% confidence level, the uncertainties of particle counting and sizing for the TDMPS are estimated to 10% and 5%, respectively, and the respective uncertainties for APS are 10% and 9% (Wex, 2002).

2.4. Size-segregated aerosol mass and chemical compositions

From 297 to 304 DOY 2004, a 10-stage Micro-Orifice Uniform Deposit Impactor (MOUDI, MSP Corporation, Minneapolis, Miilmesota, USA, Model 110. Fifty percent aerodynamic cut-off diameters: 0.056/0.18/0.32/0.56/1.0/1.8/3.2/5.6/10.0/18.0 μm), located nearby the measuring container, sampled the aerosol with Aluminum foils at ambient conditions. In total, 16 samples have been taken continuously with a time interval of 12 h (daytime from 8:00 to 20:00, and nighttime from 20:00 to 8:00 of the following day). The particle mass concentrations were determined gravimetrically at 20 °C and RH of 52%. Elemental carbon (EC) and organic carbon (OC) were analyzed by a two-step thermographic method, using a Carbon Analyzer (Ströhlein, Model C-mat 550). The mass concentrations of anions (Cl^-, NO_3^-, SO_4^{2-}) were measured with capillary zone electrophoresis using a Spectra Phoresis instrument (CE, Thermo, Inc., Waltham, MA, USA), while cations (NH_4^+, Na^+, K^+, Mg^{2+}, Ca^{2+}) were determined with ion chromatography (IC, Metron, Switzerland).

In addition, a Steam Jet Aerosol Collector (SJAC, ECN, Netherlands) system (Slanina et al., 2001) has been used at Xinken, continuously measuring the major aerosol water soluble chemical compositions in $PM_{2.5}$, with a time resolution of 30 min (Hu et al., 2008). Routine gas phase observations were also available (Su et al., 2008), including CO, O_3, NO and NO_y.

3. Methods

In order to get insight of the chemical sources apportionment of the AOPs, the measured aerosol micro-physical and chemical properties are used to calculate the AOPs of the individual aerosol chemical components for sub-1 μm ($D_{p,Stokes} \leqslant 1$ μm), super-1 μm ($1\ \mu m < D_{p,Stokes} < 10\ \mu m$) and sub-10 μm ($D_{p,Stokes} \leqslant 10$ μm) particles at dry conditions. The contribution of water uptake has been taking into account too.

As mentioned before, the MOUDI sampled at ambient RH in the field, and the filters were gravimetrically weight at RH 52% in the lab. The water fractions at each MOUDI stage were determined based on the measured particle number size distributions at dry conditions and the size-segregated particle growth factors at ambient and RH 52% (Eichler et al., 2008). Consequently, the dry aerosol mass in each stage can be calculated by subtracting the water mass.

The chemical components considered in later optical calculations are sea salt (SS), non-sea-salt sulfate (nss-sulfate), nitrate, particulate organic matter (POM), EC and residual. POM are determined by multiplying measured OC (μg cm^{-3}) by a POM factor of 1.4. This POM factor, average of the molecular weight per carbon weight for the organic aerosol, is assumed based on a review of published measurements of the composition of organic aerosol in urban and non-urban regions (Turpin and Lim, 2001). By assuming the electrical charge neutrality, Eichler et al. (2008) apportions the ionic species on each impactor stage to salts commonly found in the atmosphere. It assumes that all measured Na^+ are derived from sea salts, calculated with $[\text{sea salt}] = [Cl^-] + [Na^+] \times 1.47$. Here, 1.47 is the seawater ratio of the total mass concentration of Na^+, K^+, Mg^{2+}, Ca^{2+}, SO_4^{2-} and HCO_3^- to Na^+ (Holland, 1978). This approach prevents the inclusion of non-sea-salt K^+, Mg^{2+}, Ca^{2+}, SO_4^{2-} and HCO_3^- in the sea salt and allows for the loss of Cl^- depletion process (Quinn et al., 2000). The mass concentration of nss-sulfate is found by summing up $(NH_4)_2SO_4$, NH_4HSO_4, H_2SO_4, and K_2SO_4. Nitrate, including NH_4NO_3, $NaNO_3$ and KNO_3, is

Please cite this article as: Cheng, Y.F., et al., Aerosol optical properties and related chemical apportionment at Xinken in Pearl River Delta of China. Atmospheric Environment (2008), doi:10.1016/j.atmosenv.2008.02.034

also taken into account in the chemical apportionment since it is considered to be an important aerosol species for atmospheric chemistry in China (Zhang et al., 2004). Other than sea salts, nss-sulfate, nitrate, POM and EC, the rest of the dry aerosol mass is named as "residual". In the super-1 μm range, the residual is mainly considered as soil dust and/or fly ash. However, it is worth to point out that there is also considerable amount of residual in the sub-1 μm range (Liu et al., 2008a,b).

According to the open literature (McGraw-Hill, 1928; HOCP, 1963; Egan and Hilgeman, 1980; Ouimette and Flagan, 1982; Hasan and Dzubay, 1983; Kent et al., 1983; Hänel, 1987; Covert et al., 1990; d' Almeida et al., 1991; Sloane et al., 1991; Tang and Munkelwitz, 1994; Seinfeld and Pandis, 1998; Redemann et al., 2000; Mallet et al., 2003; Bond and Bergstrom, 2006; Hoffer et al., 2006; Schkolnik et al., 2007 etc.), the assumed density and $\tilde{m}$ of each chemical component are presented in Table 1. For each MOUDI stage, the aerosol densities at ambient conditions are calculated with the densities of dry masses of chemical components and water mass at ambient RH. Accordingly, the Stokes cut-off diameters can be calculated by using the aerodynamic ones divided by the square root of the ambient aerosol densities (Seinfeld and Pandis, 1998).

Internal and external mixture (Bohren and Huffman, 1998) of all the chemical components can be treated separately in the Mie calculations. Lesins et al. (2002) indicated that the optical equilibrium $\tilde{m}$ were insensitive to the choice of mixing rule with the largest percentage deviations occurring for small mass fractions of EC inclusions (10% EC in aerosol mass), and the effect on the AOPs was typically less than 1%. Hence, optical equilibrium $\tilde{m}$ for internal mixture is derived as a simple volume-average mixture among the $\tilde{m}$ of those six chemical components for each impactor stage. For the external mixture, the number size distributions of each chemical component is partitioned with a volume weighting from the total number size distributions (Quinn et al., 1995; Cheng et al., 2006). To support this methods, closure studies of the size-segregated chemical, gravimetric and number distribution-derived aerosol mass at Xinken has been done by Cheng et al. (2008, in preparation) and they agree within the reasonable uncertainty ranges. In the Mie calculation, not only the $\sigma_{ep;sp;ap}$ but also the asymmetry parameter (g) can be calculated with $g = \int_0^{\pi} \overline{S}\cos(\theta)\,d\theta / \int_0^{\pi} \overline{S}\sin(\theta)\,d\theta$. Here, $\overline{S}$ is the scattering phase function.

The uncertainty of these Mie calculations due to the uncertainties of experiments and assumptions has been evaluated by a Monte Carlo sensitivity study (Cheng et al., 2006). At 99% confidence level, the overall uncertainties in the simulations of σ_{ep}, σ_{sp} and σ_{ap} are 7%, 8% and 12% for external mixture, respectively, and 8%, 9% and 15% for internal mixture.

Table 1
Densities and complex refractive indices of different aerosol chemical compositions used in the Mie calculations

	Density ($g\,cm^{-3}$)	Refractive index
Sea salt	2.0	$1.54 - 10^{-7}i$
Nitrate	1.725	$1.54 - 10^{-7}i$
nss-Sulfate[a]	1.748	$1.54 - 10^{-7}i$
POM[b]	1.4	$1.55 - 0.001i$
EC[c]	1.5	$1.80 - 0.54i$
Residual	2.0	$1.58 - 0.005i$

[a]Non-sea-salt sulfate.
[b]Particulate organic matter.
[c]Elemental carbon.

4. Results and discussion

4.1. Overview of the aerosol optical properties

Winter and fall are generally considered to be the most polluted seasons in the PRD area (Man and Shih, 2001; Louie et al., 2005). In the ground-based measurements, a significant rise in σ_{sp} or σ_{ap} is identified as an "episode". It satisfies the requirement that the rise of σ_{sp} or σ_{ap} lasted for one or more consecutive hours and exceeded three standard deviations of the overall mean. Accordingly, there were four episodes occurring around 280–286, 291–292, 298–299 and 306 DOY 2004 during the field campaign (Figs. 3a and c). In Hong Kong of the same area, three to four times of such synoptic-related episodes during October or November in the former years have also been reported (Man and Shih, 2001).

Time series (15 min) of the AOPs for the sub-10 μm particles at dry conditions are plotted in Fig. 3. Table 2 summarizes the relevant statistic information during the campaign (278–310 DOY). The mean values of $\sigma_{sp,550\,nm}$ and $\sigma_{ap,50\,nm}$ are 333 ± 137 and $70 \pm 42\,Mm^{-1}$, and their maximum values can reach up to 958 and $227\,Mm^{-1}$, respectively. $\sigma_{sp,550\,nm}$ and $\sigma_{ap,550\,nm}$ at Xinken are much more

Please cite this article as: Cheng, Y.F., et al., Aerosol optical properties and related chemical apportionment at Xinken in Pearl River Delta of China. Atmospheric Environment (2008), doi:10.1016/j.atmosenv.2008.02.034

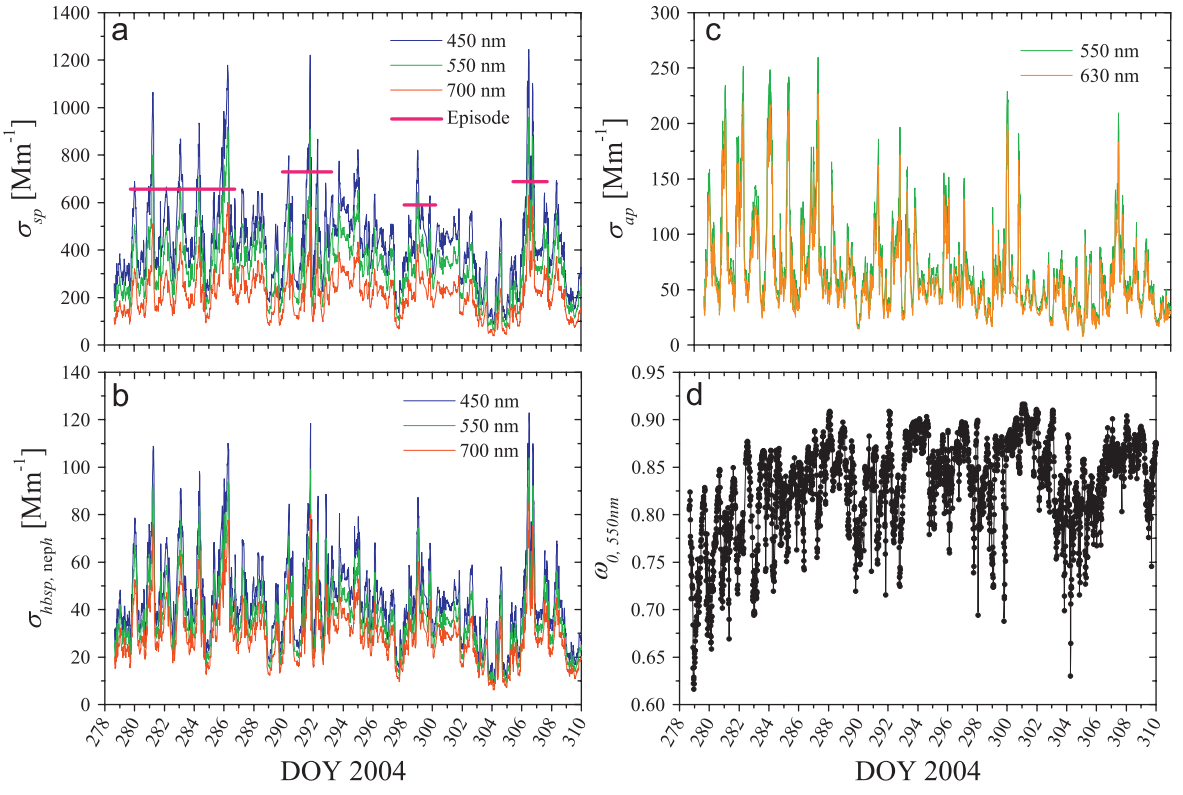

Fig. 3. Complete time series (15 min) of the measured dry aerosol optical properties (RH < 20%) at Xinken in Pearl River Delta of China from 278 to 310 DOY 2004. (a) The corrected total scattering coefficient (σ_{sp}), (b) hemispheric backscattering coefficient ($\sigma_{hbsp,neph}$), (c) absorption coefficient (σ_{ap}), and (d) single scattering albedo (ω_0).

higher than those at Cape D'Aguilar, a remote area of Hong Kong (Man and Shih, 2001), where σ_{sp} and σ_{ap} at 530 nm were 71 and 19 Mm^{-1} in the Autumn of 1997 and 1998, respectively. Compared with other rural/non-urban polluted sites in Asia, $\sigma_{sp,550\,nm}$ at Xinken is similar to the values measured at Lin'an, China ($353 \pm 202\,Mm^{-1}$) during October–December 1999, and it is only about 1.4 times higher than the Gosan, Korea ($244 \pm 123\,Mm^{-1}$) during pollution episodes in 2001 (Kim et al., 2005). However, although Xinken, Lin'an and Gosan sites are in a similar way affected by large cities, regional transport and local sources, $\sigma_{ap,550\,nm}$ in Lin'an ($23 \pm 14\,Mm^{-1}$) and Gosan ($25 \pm 13\,Mm^{-1}$) are a factor of 3–4 lower than that at Xinken. Moreover, σ_{sp} at Xinken is considerably stronger than non-urban polluted sites inNorth America and Europe including Bondville, IL, southern Great Plains, OK, Sable Island, NS, and Sagres, Portugal where $\sigma_{sp,550\,nm}$ are 30–50 Mm^{-1} (Ogren, 1995; Carrico et al., 1998, 2000; Koloutsou-Vakakis et al., 2001; Carrico et al., 2003). And it is also higher than the non-urban sites in southeast United Sates including the IMPROVE sites of Shenandoah and Great Smokies where annual average ambient total σ_{sp} range from 100 to 125 Mm^{-1} (Malm et al., 1994). In addition, $\sigma_{sp,550\,nm}$ and $\sigma_{ap,550\,nm}$ at Xinken is a factor of 3 higher than the city/urban cite in Atlanta, USA (121 ± 48 and $16 \pm 12\,Mm^{-1}$) during the 1999 Atlanta Supersite Experiment (Carrico et al., 2003), but only slightly lower than the mean values of Beijing, China (488 ± 370 and $83 \pm 40\,Mm^{-1}$) in 1999 (Bergin et al., 2001), which means that Xinken is at the same pollution level as in Beijing in 1999. While during January 2005, $\sigma_{sp,550\,nm}$ and $\sigma_{ap,550\,nm}$ in Beijing has been found to be at a even higher level of 777 ± 689 and $89 \pm 74\,Mm^{-1}$, respectively (Heintzenberg et al., 2008).

An estimation of the single scattering albedo at Xinken is $\omega_{0,550\,nm} = 0.83 \pm 0.05$ (Fig. 3d), which is considerably low. However, it is important to clarify

Please cite this article as: Cheng, Y.F., et al., Aerosol optical properties and related chemical apportionment at Xinken in Pearl River Delta of China. Atmospheric Environment (2008), doi:10.1016/j.atmosenv.2008.02.034

Table 2
Average and extreme values of the extensive and intensive aerosol optical properties at dry conditions (RH < 20%) at Xinken in Pearl River Delta of China 2004 (Here 2945 data points (15 min) are evaluated)

		Means	Std	COV	Max	Min
Extensive optical properties						
σ_{sp} (Mm^{-1})	450 nm	436	175	41	1250	87
	550 nm	333	137	41	958	62
	700 nm	215	91	43	629	38
σ_{hbsp} (Mm^{-1})	450 nm	44	17	41	123	9
	550 nm	37	15	41	104	8
	700 nm	29	12	41	85	6
σ_{ap} (Mm^{-1})	550 nm	70	42	60	260	9
	630 nm	61	37	61	227	8
L_v (km)	550 nm	5.3	2.5	47	19.6	1.1
Intensive optical properties						
ω_0	550 nm	0.83	0.05	6	0.92	0.62
$\beta(1)$ (%)	550 nm	11	1	9	15	9
$\mathring{a}$	450–700 nm	1.6	0.15	9	2.0	1.2
g	550 nm	0.67	0.01	1	0.69	0.64

that ω_0 of 0.83 is for the dry particles at RH < 20%, while the influence of higher ambient RH would result in higher ω_0 (Cheng et al., 2008). From the open literature, ω_0 in mid-visible wavelength range varies from 0.79 (freshly produced aerosol from biomass burning) (Reid et al., 1998) to 0.99 (clean marine aerosol) (Carrico et al., 2003) with different environment circumstances, aerosol sources and age (Bodhaine, 1995; Reid et al., 1998; Carrico et al., 2000, 2003; Bergin et al., 2001; Kim et al., 2005). Compared to the ω_0 of regional hazes dominated by smoke in Brazil (Reid et al., 1998), ω_0 at Xinken is similar to that of the relatively young smoke from forest and slash burning in Marabá (0.83 ± 0.02). In Atlanta (USA) and Gosan (Korea), ω_0 were found to be 0.87 ± 0.08 and 0.88 ± 0.02, respectively, which are 5% higher than that at Xinken. However, ω_0 in Beijing in 1999 was reported to be even lower with a value of 0.81 ± 0.08 (Bergin et al., 2001); while during January 2005, ω_0 in Beijing was determined to be 0.84 ± 0.03 (Heintzenberg et al., 2008), which is comparable with Xinken. In a word, although σ_{ep} at Xinken is dominated by σ_{sp}, σ_{ap} also make a substantial (17%) contribution to σ_{ep}. This results at Xinken much more closely reflect an urban core than even a polluted rural site.

The Ångström exponent $\mathring{a}_{450/700}$ at Xinken is about 1.6, and the average effective particle

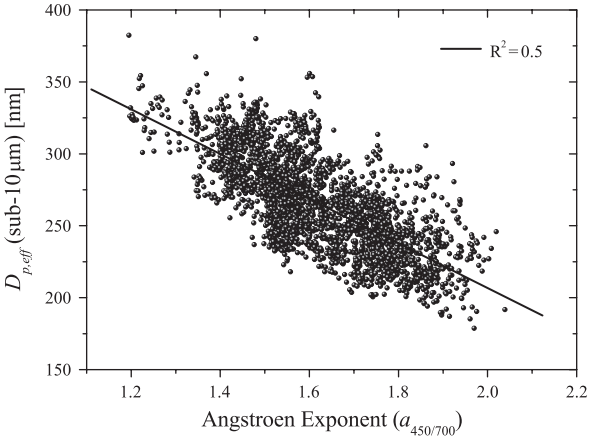

Fig. 4. Linear correlation between the Ångström exponent ($\mathring{a}_{450/700}$, presented as "Angstrom exponent ($a_{450/700}$)" in the figure) and the effective particle diameter ($D_{p,eff}$) of the sub-10 μm particles, with relative correlation coefficient (R^2) of 0.5.

diameter ($D_{p,eff}$) of sub-10 μm particles is about 250 nm. $D_{p,eff}$ is calculated with $D_{p,eff} = \int n(D_p) D_p^3 \, dD_p / \int n(D_p) D_p^2 \, dD_p$. Here, $n(D_p)$ is the dry particle number is distribution and D_p is particle diameter. A strong anti-correlation with $R^2 = 0.5$ has been found between $\mathring{a}_{450/700}$ and $D_{p,eff}$, as shown in Fig. 4. The average $\beta(1)$ and g are about 11% and 0.67 at 550 nm, respectively, without obvious temporal variation. During ACE-1, $\beta(1)$ were found to be $16 \pm 1\%$ at RH 22% and $12 \pm 3\%$ at RH 82% at a southern hemisphere site, Cape Grim of Tasmania (Carrico et al., 1998). During ACE-2, Carrico et al. (2000) reported $\beta(1)$ at Sagres of Portugal to be about 12%. However, $\beta(1)$ for the particle size parameter within the Mie regime is typically about 10% (Lelieveld and Heintzenberg, 1992). The differences in $\beta(1)$ of Sagres, Xinken and Mie theory prediction are not significant and generally show the same values for polluted sites, as compared to background marine sites.

Visibility at Xinken is estimated about 5.3 ± 2.5 km which is rather low. However, the water taken up by the particle should be taken into account, L_v at Xinken under ambient conditions could be even lower. From 16 October to 3 November 2003, the average L_v at ambient RH in Guangzhou, which has been converted to the upper limit visibility with the modified Koschmieder constant 1.9, is about 5 km and the lowest value is less than 1 km (Wu et al., 2005). The low L_v at Xinken is consistent with high aerosol mass and number concentrations in the sub-micrometer range

Please cite this article as: Cheng, Y.F., et al., Aerosol optical properties and related chemical apportionment at Xinken in Pearl River Delta of China. Atmospheric Environment (2008), doi:10.1016/j.atmosenv.2008.02.034

(Liu et al., 2008b), which are also clearly seen in the results of Raman LIDAR and Sun photometry measurements (Ansmann et al., 2005). The high aerosol light extinction, scattering and absorption coefficients, as well as low visibility, in this region suggest the presence of a regional haze in the PRD area of the Southeastern China.

4.2. Variation of the aerosol optical properties

Although the optical measurements were conducted at the dry conditions, and also the stagnant synoptic meteorology condition dominated, the AOPs measured at Xinken demonstrate large variability over timescales ranging from minutes to days (Fig. 3). The coefficient of variation (COV = s/means) can be used to compare the variability of different data sets. As shown in Table 2, extensive AOPs show much greater variability (COV~40%) than intensive properties (COV <10%). The lower variability in aerosol intensive properties suggests that their controlling influences such as aerosol size distribution patterns, relative chemical compositions, and particle morphology had variabilities being less important to aerosol radiative properties than changes in fine particle mass and number concentrations (Carrico et al., 2003).

4.2.1. Systematic relationship

Knowledge concerning systematic relationships among AOPs is useful in reducing uncertainties in remote sensing data because it can be used to make better assumptions about unknown aerosol properties (Delene and Ogren, 2002). Remer and Kaufman (1998) have illustrated the importance of using a dynamic model in which aerosol properties vary with aerosol load for the inversion of remote sensing data. Since then, some attempts have been made to trace the possible factors which influence or govern the variability of the AOPs at Xinken. During the whole period, only the time series of σ_{sp}, $\sigma_{hbsp,neph}$ and σ_{ap} fairly follow each other (Figs. 3a–c and 5a). However, for the other variables, simple correlations do not exist between any of those extensive and intensive properties, and no single one of them was a dominating controlling factor, especially during the calm wind period (Figs. 5b–d and 6). It implies that the aerosols at Xinken are rather complicated concerning sources, chemical compositions and aging.

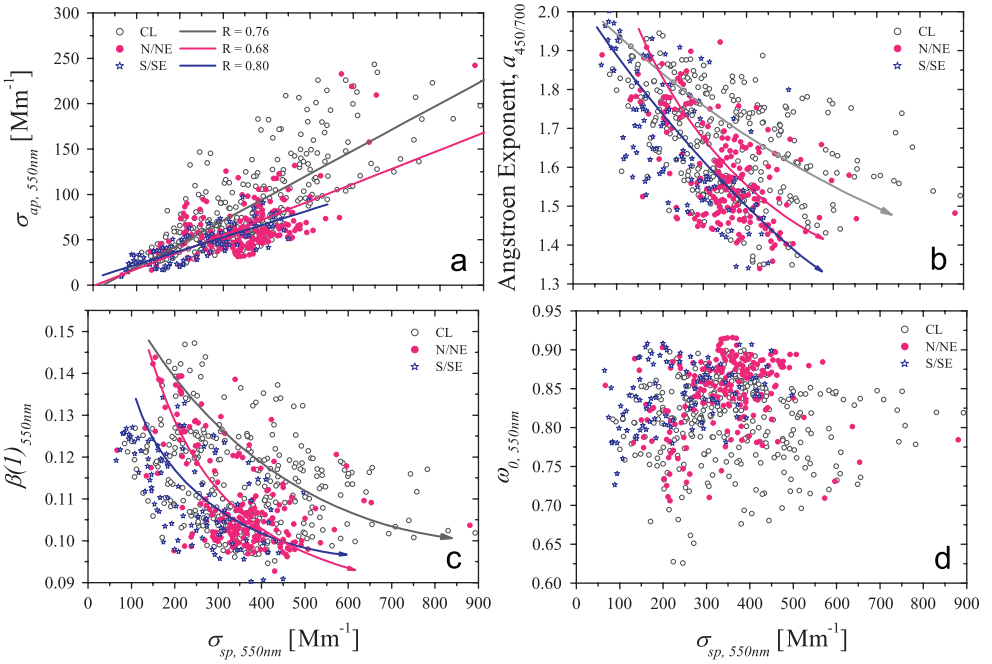

Fig. 5. Relationships among the various aerosol optical properties, including scattering and absorption coefficients ($\sigma_{sp;ap,550\,nm}$), Ångström exponent ($\mathring{a}_{450/700}$, presented as "Angstrom exponent ($a_{450/700}$)" in the figure), single scattering albedo ($\omega_{0,550\,nm}$) and hemispheric backscattering fraction ($\beta(1)_{550\,nm}$). The data sets are sorted with the three wind patterns, calm wind (CL), north/northeast wind (N/NE) and south/southeast wind (S/SE). The time resolution of the data sets is 1 h.

Please cite this article as: Cheng, Y.F., et al., Aerosol optical properties and related chemical apportionment at Xinken in Pearl River Delta of China. Atmospheric Environment (2008), doi:10.1016/j.atmosenv.2008.02.034

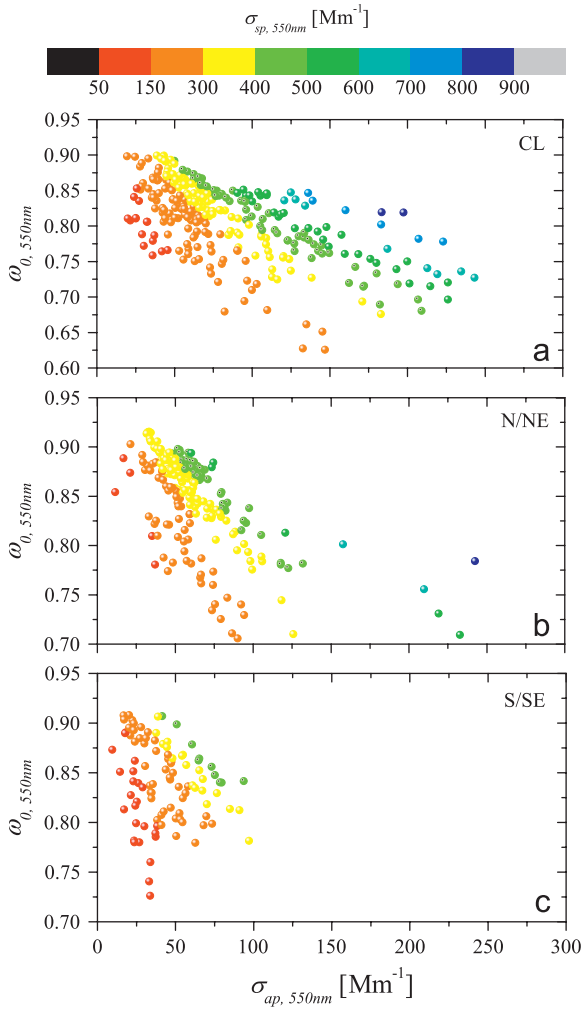

Fig. 6. Relationships between absorption coefficient ($\sigma_{ap,550\,nm}$) and single scattering albedo ($\omega_{0,550\,nm}$) for the three wind patterns, calm wind (CL), north/northeast wind (N/NE) and south/southeast wind (S/SE). The data sets are sorted with the scattering coefficient ($\sigma_{sp,550\,nm}$). The time resolution of the data sets is 1 h.

The data sets are averaged to 1 h to exclude the influences by the extreme values and classified according to the three different wind patterns (CL, N/NE and S/SE). Figs. 5 and 6 present the complex relationship among the intensive AOPs ($\sigma_{ap,550\,nm}$, $\mathring{a}_{450/700}$, $\beta(1)_{550\,nm}$ and $\omega_{0,550\,nm}$) and the aerosol load (represented by $\sigma_{sp,550\,nm}$). As shown in Fig. 5b, $\mathring{a}$ decreases with increasing σ_{sp}, that is, the higher the aerosol load, the more contribution to the σ_{sp} by the relatively bigger particles, although they are still within the fine particle range. This is consistent with the $\beta(1)$–σ_{sp} relationship (Fig. 5c), since the bigger particle scatter more light to the forward direction (Bohren and Huffman, 1998). These may hint at the regionality of the pollution problem at Xinken, as somewhat more aged aerosols (relative larger D_p) rather than fresh emission (smaller D_p) are associated with episodes. These relationships were also found in the study of Delene and Ogren (2002). However, all those aforementioned relationships are not very pronounced during the CL period.

Theoretically, the variational trend in ω_0 ($\Delta\omega_0$) is controlled by the signs of $(\sigma_{ap}\cdot\Delta\sigma_{sp}-\sigma_{sp}\cdot\Delta\sigma_{ap})$ and $(\sigma_{ep}+\Delta\sigma_{ep})$, shown as

$$\Delta\omega_0=\frac{\sigma_{ap}\cdot\Delta\sigma_{sp}-\sigma_{sp}\cdot\Delta\sigma_{ap}}{(\sigma_{ep}+\Delta\sigma_{ep})\cdot\sigma_{ep}}. \quad (1)$$

In contrast to Delene and Ogren (2002) and Kim et al. (2005) who found that ω_0 increased with increasing σ_{sp} or σ_{ep} for typical polluted continental aged aerosols), there is no pronounced relationship between ω_0 and σ_{sp} at Xinken, especially during the CL period (Fig. 5d). However, it has been found in Fig. 6 that ω_0 generally decreases with increasing σ_{ap}, even though σ_{sp} and σ_{ap} mostly show the same trend. This indicates that $\Delta\omega_0$ is more sensitive to $\Delta\sigma_{ap}$ than to $\Delta\sigma_{sp}$ at Xinken. On one hand, the decreasing rate of ω_0 is smaller when the aerosol load (σ_{sp}) is higher. On the other hand, for the same level of aerosol load, the decreasing rate of ω_0 is greatest during S/SE period, followed by N/NE and then CL periods. These may due to two reasons. First, when the aerosol pollution is increasing the mass ratio of light-scattering materials (e.g., sulfate and most of the OC) gets higher. Second, the EC mixing state may differ during those three different wind patterns. Because for the same amount of EC, more internal mixture in a more aged air mass leads to greater absorption capacity of the EC (Jacobson, 2001) and hence faster decreasing of ω_0. The second reason has been confirmed by Cheng et al. (2006). They found that, at Xinken, there was more internally mixed EC during S/SE period, which may be influenced by the aged air mass coming from the sea, and then followed by N/NE period, during which aerosol is mainly transported from the continental urban area. They also indicate that during CL, the EC was mostly locally and freshly produced and hence almost all was externally mixed.

4.2.2. Diurnal variation

The time-scale and nature of the measured variability is also revealed by autocorrelation analysis (Fig. 2b). The diurnal variation of σ_{ap}

Please cite this article as: Cheng, Y.F., et al., Aerosol optical properties and related chemical apportionment at Xinken in Pearl River Delta of China. Atmospheric Environment (2008), doi:10.1016/j.atmosenv.2008.02.034

(correlation coefficient R~0.4 at 24 h) is stronger than that of σ_{sp} (R~0.2 at 24 h). Two peaks (R~0.4 at 12 h and R~0.55 at 24 h) have been found in the variation pattern of ω_0. Such trends are linked to both the diel emission trends and meteorological factors such as the diurnal variation of the planet boundary layer (PBL) height and wind patterns.

Therefore, the diurnal variations of median values (to avoid the influence of extreme outliers) of AOPs (15 min data) are presented in Fig. 7 for the three wind patterns. As shown in the wind frequency of Fig. 7a, the S/SE winds nearly only occur during nighttime (mostly started at around 20:00). The maximum values of σ_{sp} and σ_{ap} (15 min) mostly happen during CL winds.This can be seen by comparing Figs. 1a and 3a. Also, as shown in the hourly averaged values of Fig. 5a, the high values of σ_{sp} and σ_{ap} are mainly found in the "gray circles" for the CL pattern. However, if looking at the median values in Figs. 7e and f, there are no significant differences in σ_{sp} during CL and N/NE, and the highest median values in Fig. 7e occur during N/NE winds between 20:00 and 24:00. The median pollution level in nighttime is lower during S/SE winds.

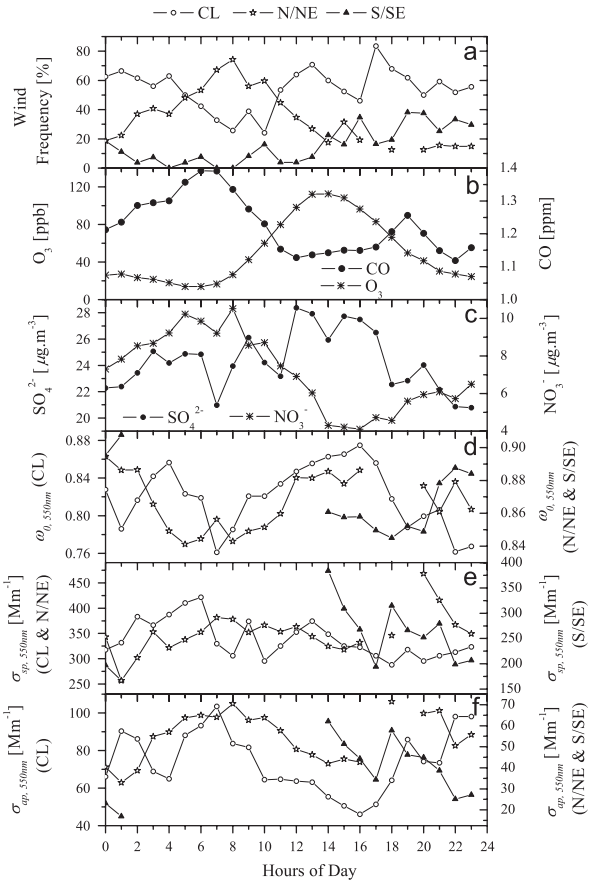

Fig. 7. Diurnal variations of various chemical and optical properties in gas and aerosol phases. The data sets are sorted with the three wind patterns, calm wind (CL), north/northeast wind (N/NE) and south/southeast wind (S/SE).

The first peaks of σ_{ap} during CL and N/NE winds both occur at around 6:00–9:00, and the second peaks are at around 19:00 to midnight. During N/NE winds, the influences of PBL development on the diurnal variation of σ_{sp} are not very clear, with only one significant peak at around 22:00. The peaks of σ_{sp} during CL winds are found in the early morning and afternoon. The variations of ω_0 during N/NE and S/SE wind are similar, but different to that during CL winds. This may due to that the aerosol particles both experience transportation during N/NE and S/SE winds, while the particles were freshly produced from local sources and accumulated in CL winds.

Since PBL height generally varies with surface T, the diurnal variation of σ_{sp} and σ_{ap} can likely be explained in part by changes in PBL. However, ω_0 also show diurnal variation as shown in the auto-correlation, reflecting the different degree of the peak-to-trough diel variation in σ_{sp} and σ_{ap}. This suggests that the diurnal variation of σ_{sp} and σ_{ap} cannot be solely explained by dilution as the PBL height increasing during the day. While σ_{sp} and σ_{ap} decrease from 9:00 to late afternoon following the PBL development, ω_0 increases. This indicates that the EC, generally emitted by primary sources, dilutes faster than the scattering components during the day. Following the increasing solar radiation during daytime, the photochemistry is more active and therefore produces more secondary pollutants, like sulfate (Fig. 7c) which is one of the major scattering chemical compounds in particles. During nighttime of N/NE and S/SE winds and also around 4:00 of CL winds, there are the secondary peaks in ω_0, This may be explained by the decreasing of combustion sources of EC, which can be also found in the decrease of CO during nighttime (Fig. 7b). On the other hand, the O_3 which does not reach 0 during nighttime at Xinken. Through the nighttime chemistry, especially under high RH conditions during the nights of S/SE periods, the formation of ammonium nitrate may contribute to σ_{sp} (Fig. 7b) and thereby contribute to an increase in ω_0. This assumption is proved by the optical related chemical apportionment at Xinken and will be discussed later. Bergin et al. (2001) has also found that

Please cite this article as: Cheng, Y.F., et al., Aerosol optical properties and related chemical apportionment at Xinken in Pearl River Delta of China. Atmospheric Environment (2008), doi:10.1016/j.atmosenv.2008.02.034

the nitrate contribution to σ_{sp} increased during nighttime in Beijing. However, as discussed in Section 4.2.1, $\Delta\omega_0$ is more sensitive to $\Delta\sigma_{ap}$. In the early morning and around 6:00–7:00 during CL winds, there are two troughs in ω_0 diurnal pattern, accompanying with significant increases of σ_{ap} and CO (Figs. 7b, d and f). This indicates that there may be strong local combustion activities around the time. Similar pattern of CO have been also observed in Guangzhou urban site (Andreae et al., 2008) for the period, which mainly contributed by the traffic rush incidence. Even though traffic on the main road leading to Xinken was not dense and therefore did probably not contribute significantly to the local air pollution, again showing this at Xinken to be similar to highly urban areas, is merited in light of the pollution regionality in PRD.

4.3. Chemical apportionment of the aerosol optical properties

The "measured" extinction coefficient ($\sigma_{ep,e,550\,nm}$) at 550 nm for sub-10 μm particles is derived from summing up the $\sigma_{sp,e,550\,nm}$ and $\sigma_{ap,e,550\,nm}$. At 99% confidence level, the uncertainty of $\sigma_{ep,e,550\,nm}$ is estimated as 6% by a simple Monte Carlo simulation with the uncertainties of nephelometer and MAAP. Under dry conditions, $\sigma_{ep,Mie,550\,nm}$ for the external and internal mixtures have been simulated based on the measured size-segregated chemical compositions and dry particle number size distributions, as described in Section 3. As a whole, the measured and calculated $\sigma_{ep,550\,nm}$ agree within the overall experimental and calculating uncertainties (Fig. 8). There are no obvious differences between the modeled $\sigma_{ep,Mie,550\,nm}$ of external and internal mixtures. The same mixture-independence of the simulated σ_{ep} has been reported by Ackerman and Toon (1981), Pesava et al. (2001), Eldering et al. (2002), Wex (2002) and Cheng et al. (2006).

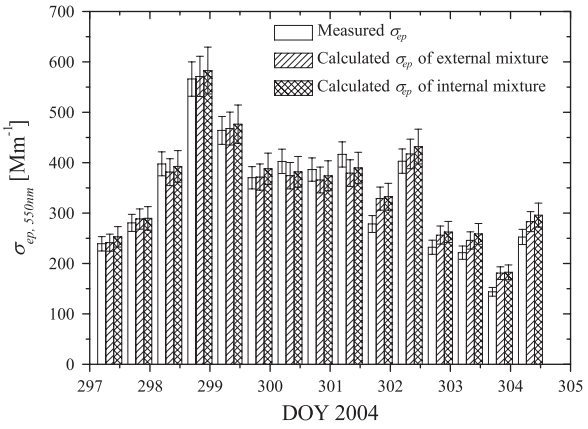

Fig. 8. Comparison of measured extinction coefficients ($\sigma_{ep,550\,nm}$) and calculated ones for external and internal mixtures, as well as the uncertainties of experiment and calculations at 99% confidence level derived from the Monte Carlo simulations.

4.3.1. Fractional contribution to extinction coefficient

The fractional contributions of the major particle chemical compositions to aerosol extinction ($f_{ep,i,550\,nm}$) are calculated with an external mixture under the dry conditions (RH < 20%). The results are shown in Fig. 9b. The chemical components (i) considered here are sea salt, nss-sulfate, nitrate, POM, EC and residual. Using the external mixture is to distinguish the $f_{ep;sp;ap,i}$ of different chemical compositions, which cannot be done with internal or other mixtures. As shown in Figs. 9b and c, the trend of $f_{ep,dry,i}$ for each of the chemical compositions generally follows the trend of their sub-1 μm mass fractions ($f_{mass,dry,i}$).

The greatest $f_{ep,dry}$ is from nss-sulfate with 44±6% due to the highest $f_{mass,dry}$ of nss-sulfate at Xinken. During the Aerosols99 cruise across the Atlantic, Quinn et al. (2001) indicated that nss-sulfate had the highest contribution to σ_{ep} within the sub-1 μm range in the North American air mass region ($45 \pm 30\%$ at RH 55%), resulting from emission from the east coast of the United States. During INDOEX 1999, the region impacted by lower-level flow from Arabia, Arabia/Indian subcontinent had a high mean sub-1 μm f_{ep} of $55 \pm 19\%$ due to sulfate at RH 55% (Quinn et al., 2002), which is also comparable with our results.

The carbonaceous species, POM and EC both contribute about 17% to $\sigma_{ep,dry}$ at Xinken. Comparably, $f_{ep,POM}$ of ~18–23% were reported by Quinn et al. (2002) for both marine and continentally influenced air mass regions. EC is well-known with not only its light absorption property but also great extinction capacity. While, $f_{ep,EC}$ varies as function of location. It has been found to be $6.4 \pm 2.7\%$ in biomass burning region in 1999 Atlantic cruise, and $21 \pm 7.5\%$ for the Arabian sea-coastal Indian region, but ~33% for East Indian subcontinent and Indian subcontinent region (Quinn et al., 2001, 2002). In 1981, Groblicki et al. (1981) reported that EC in fine particle can contribute as high as 37.7% to σ_{ep} in Denver. However, $f_{ep,dry,EC}$

Please cite this article as: Cheng, Y.F., et al., Aerosol optical properties and related chemical apportionment at Xinken in Pearl River Delta of China. Atmospheric Environment (2008), doi:10.1016/j.atmosenv.2008.02.034

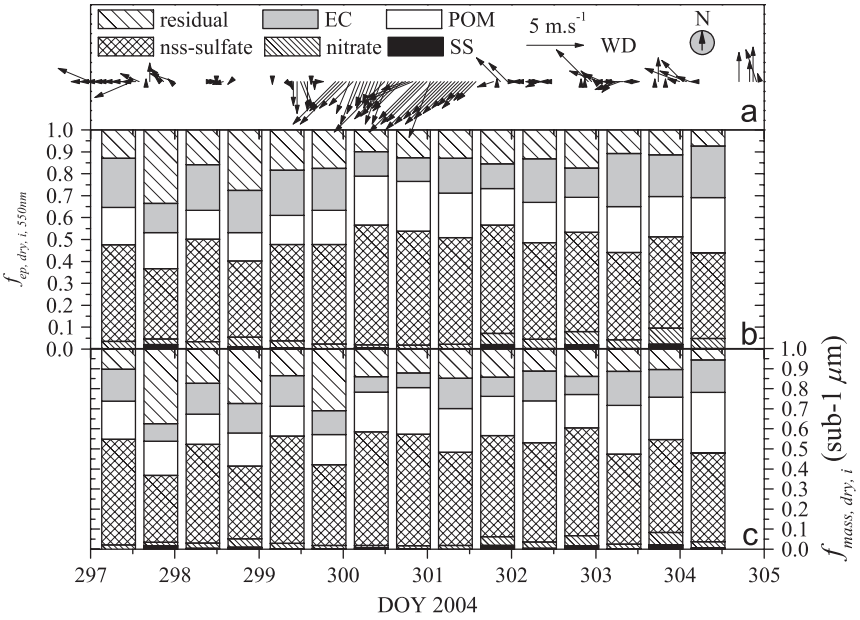

Fig. 9. Time series of the fractional contributions of sub-10 μm aerosol extinction ($f_{ep,dry,i}$) at dry conditions (RH < 20%) and of sub-1 μm particle mass ($f_{mass,i}$) due to the individual chemical compositions (i) in terms of the local wind pattern. The time resolutions of $f_{ep;mass,dry,i}$ are 12 h, with daytime from 8:00 to 20:00 and nighttime from 20:00 to 8:00 of the following day.

at Xinken lies within the reported range. At the same time, it is worth to note that concerning the impairment of visibility, the carbonaceous species (EC and POM) is comparable with the nss-sulfate. Both of them contribute around 40%. This does not support the common assumption that sulfate dominates σ_{ep} in polluted regions (White, 1990).

The residual also contributes about 15% to σ_{ep} at Xinken due to the residual mass not only in the super-1 μm but also in the sub-1 μm ranges (Figs. 9b and c). In other studies, $f_{ep,residual}$ has been found ranging from 5% to 33%, resulting from different aerosol sources (Quinn et al., 2001, 2002; Eldering et al., 2002). In addition, the average $f_{ep,dry}$ of sea salt and nitrate are less than 1% (max 2%) and 5% (max 8%), respectively, at Xinken. However, there might be some loss of ammonium nitrate during the impactor sampling, storage and shipping (Slanina et al., 2001), hence the actual contribution from nitrate can be higher than the fraction evaluated here, although it is difficult to quantify.

At Xinken, $f_{ep,dry,i}$ also vary with the local wind patterns (Figs. 9a and b). During the N/NE winds coming directly from the polluted urban area of Chinese inner continent, the nss-sulfate contribution are higher than those during CL or S/SE winds. During CL winds, biomass burning is one of the major local source at Xinken. Quinn et al. (2001) has also indicated that f_{ep} of nss-sulfate in the biomass burning region was smaller than that in the region influenced by the emission from the east coast of USA during Aerosols 1999. $f_{ep,dry,POM}$ is higher during N/NE and S/SE winds than that during CL winds. This is opposite to the trend of $f_{ep,dry,EC}$. $f_{ep,dry,SS}$ increases during the night with S/SE winds coming from the sea. Also $f_{ep,dry,nitrate}$ increases in the nighttime during S/SE and CL winds, which may be due to the nighttime chemistry under the high RH conditions during those periods. There are obvious increases in $f_{ep,dry}$ of the residual in the nights of 297 and 298 DOY, accompanied with the significant increase of $f_{mass,dry,residual}$ in the sub-micrometer range. This results in a relative low $f_{ep,dry}$ of nss-sulfate.

It has been well-known that the water soluble aerosol compositions can take up water from the ambient atmosphere (Tang and Munkelwitz, 1993, 1994; Seinfeld and Pandis, 1998). This process alters the particle number size distributions and the refractive indices (Covert et al., 1972; Charlson et al., 1992; Tang, 1996), the key parameters governing the AOPs. The RH dependence of AOPs at Xinken has been investigated based on the dry aerosol physical and chemical properties and

Please cite this article as: Cheng, Y.F., et al., Aerosol optical properties and related chemical apportionment at Xinken in Pearl River Delta of China. Atmospheric Environment (2008), doi:10.1016/j.atmosenv.2008.02.034

particle hygroscopic behavior, and the detail can be found in Cheng et al. (2008). At RH 90%, the water can contribute up to 50–60% of $\sigma_{ep,550\,nm}$ (Fig. 10c). Consequently, $f_{ep,sulfate}(90\%)$ is only ~20%, followed by the carbonaceous of ~18%. $f_{ep,i}$(Ambient RH) are also present in Fig. 10b according to the 12 h average ambient RH (Fig. 10a). At Xinken, the average RH during daytime is $53 \pm 15\%$ (25–95%), and the corresponding water taken up contributes $10 \pm 8\%$ to $\sigma_{ep,550\,nm}$. While the average RH during nighttime is $76 \pm 12\%$ and it can reach up to around 100%. Consequently, $f_{ep,water,550\,nm}$ in the night is $\sim 30 \pm 15\%$. So, the water taken up by the particles can lead to great visibility impairment at Xinken, especially during the days with high RH.

4.3.2. Fractional contribution to scattering and absorption coefficients

The detailed closure study of the dry σ_{ep} and σ_{ap} at Xinken can be found in Cheng et al. (2006). Here, the fractional contributions of σ_{sp} and σ_{ap} due to major aerosol chemical components ($f_{sp;ap,dry,i,550\,nm}$) are shown in Figs. 11a and b. Because about half of the EC extinction is due to its light absorption, compared with the $f_{ep,dry,i}$, $f_{sp,dry,i}$ due to all the other chemical components increase, however, $f_{sp,dry,EC}$ decreases.

Sea salt, nitrate and nss-sulfate only scatter the light at 550 nm, and they do not contribute to σ_{ap}. Dust is generally considered to be the second light absorbers and also it is found that some OC can also contribute to σ_{ap} (Andreae and Gelencsèr, 2006). The imaginary parts of $\tilde{m}$ for POM and residual are assumed to be 0.001 (Hasan and Dzubay, 1983; Hoffer et al., 2006; Sloane et al., 1991; Schkolnik et al., 2007, etc.) and 0.005 (Hasan and Dzubay, 1983; Kent et al., 1983; Hänel, 1987; Sloane et al., 1991; Tang and Munkelwitz, 1994; Redemann et al., 2000 etc.), respectively. However, it is difficult to quantify the uncertainties of this assumption. From the Mie calculations, $f_{ap,dry}$ due to EC is ~91%. POM contributes less than 2%, but $f_{ap,dry,residual}$ is about 7%. A good linear correlation between σ_{ap} and EC mass concentration has been found (Fig. 12a) with a correlation coefficient R^2 of 0.92, which means that σ_{ap} can be mostly explained by EC, and this is also consistent with the chemical apportionment.

The variation of $f_{sp;ap,dry,i}$ due to individual chemical components in terms of the wind patterns are similar to $f_{ep,dry,i}$.

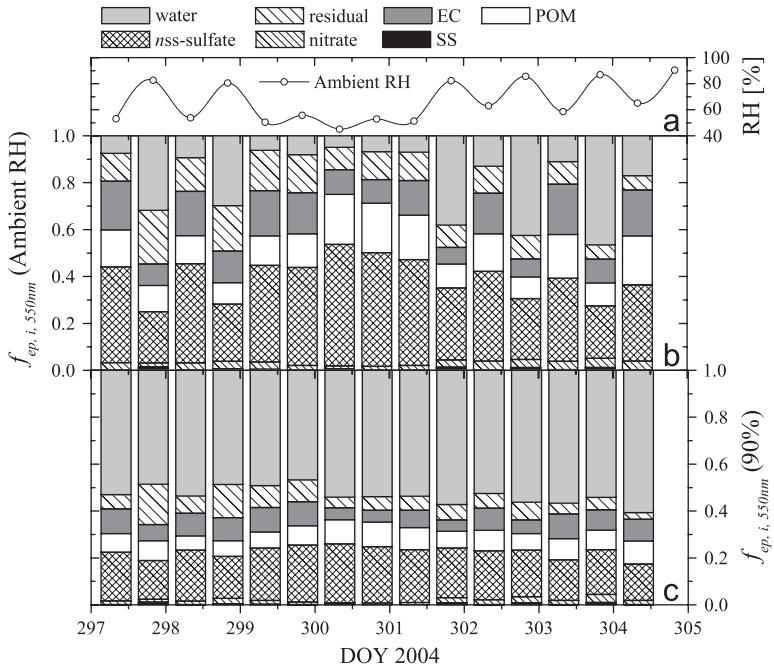

Fig. 10. Time series of the fractional contributions of sub-10 μm aerosol extinction ($f_{ep,i}$) at relative humidity (RH) of 90% and ambient RH due to the individual chemical compositions (i), including water. The time series of the ambient RH are presented in (a). The time resolutions of $f_{ep;mass,dry,i}$ are 12 h, with daytime from 8:00 to 20:00 and nighttime from 20:00 to 8:00 of the following day.

Please cite this article as: Cheng, Y.F., et al., Aerosol optical properties and related chemical apportionment at Xinken in Pearl River Delta of China. Atmospheric Environment (2008), doi:10.1016/j.atmosenv.2008.02.034

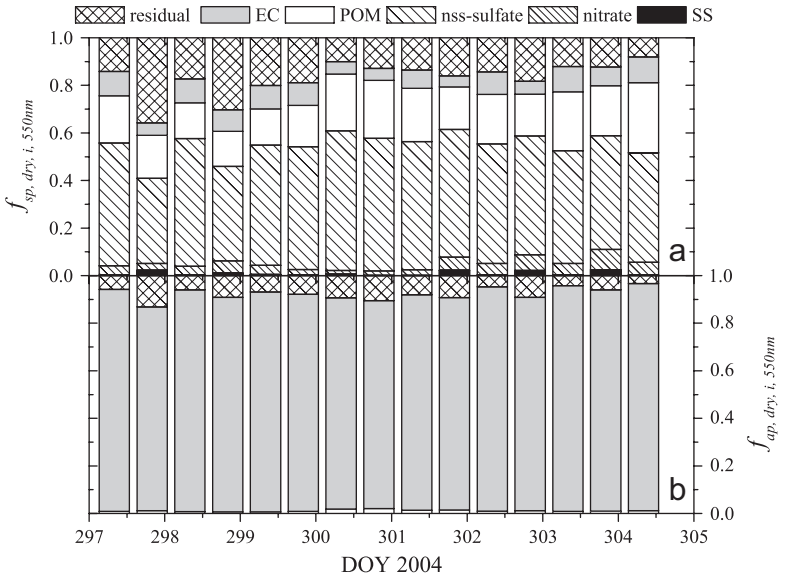

Fig. 11. Time series of the fractional contributions of sub-10 μm aerosol scattering and absorption ($f_{sp;ap,dry,i}$) at dry conditions (RH < 20%) due to the individual chemical compositions (i). The time resolutions of $f_{ep;mass,dry,i}$ are 12 h, with daytime from 8:00 to 20:00 and nighttime from 20:00 to 8:00 of the following day.

4.4. Mass extinction, scattering and absorption efficiencies

The mass extinction, scattering and absorption efficiencies ($\alpha_{ep;sp;ap,i}$) of different aerosol chemical compositions are the key parameters used to connect aerosol chemical properties and radiation model (Seinfeld and Pandis, 1998). They are defined as $\alpha_{ep;sp;ap,i} = \sigma_{ep;sp;ap,i}/m_i$. Here, m_i is the mass concentration of sub-1 μm, sub-10 μm particles, or certain chemical component i. Note that it is crucial to separate sub- and super-1 μm particles because this separates the independently varying accumulation and coarse particle mass modes which have very distinct sources, optical properties, and atmospheric lifetime (Charlson et al., 1999).

There are two basic approaches to estimating $\alpha_{ep;sp;ap,i}$: (1) application of Mie calculation based on measurements of chemical and physical size distributions and assumed $\tilde{m}$, and (2) multiple linear regression of measured AOPs against measured mass concentrations of aerosol constituents. However, a robust regression requires a large number of samples that encompass wide ranges of optical parameters, chemical component concentrations, and ratios of component concentrations. And also, to be free from systematic bias, the components included in the regression must account for all the aerosol mass, and the sample-to-sample fluctuations in optical parameters must not be correlated with fluctuations in component concentrations (Charlson et al., 1999). In our case, only 15 data sets are available, so the first approach, Mie calculation, is chosen.

4.4.1. Mass extinction, scattering and absorption efficiencies at Xinken

On the basis of the chemical apportionment for the AOPs, $\alpha_{ep;sp;ap,i,550\,nm}$ for sub-1 μm and sub-10 μm aerosol particles and individual chemical components are calculated according to the definition, summarized in Table 3. α_{ep} of sub-1 μm particles is $7.6 \pm 1.1\,m^2\,g^{-1}$, which is higher than the respective value during INDOEX 1999 ($4.0–5.6\,m^2\,g^{-1}$) (Quinn et al., 2002) and Aerosols1999 ($4.1–5.4\,m^2\,g^{-1}$) (Quinn et al., 2001). α_{ep} of sub-10 μm particles is $4.1 \pm 0.8\,m^2\,g^{-1}$, which is comparable with the respective value for Indian subcontinent ($3.7–4.7\,m^2\,g^{-1}$) (Quinn et al., 2002). α_{sp} of sub-1 μm and sub-10 μm particles are 6.4 ± 1.1 and $3.5 \pm 0.8\,m^2\,g^{-1}$, respectively. They are within the range of $PM_{2.5}$ mass scattering efficiency ($2.94–3.2\,m^2\,g^{-1}$) summarized by Waggoner and Weiss (1980), and also consistent with the Atlanta 1999 ($3.5–4.4\,m^2\,g^{-1}$) (Carrico et al., 2003).

At Xinken, α_{sp} of sub-1 μm nss-sulfate is $7.1 \pm 1.4\,m^2\,g^{-1}$ and the respective value for sub-10 μm range is $4.7 \pm 1.1\,m^2\,g^{-1}$. They are higher than those

Please cite this article as: Cheng, Y.F., et al., Aerosol optical properties and related chemical apportionment at Xinken in Pearl River Delta of China. Atmospheric Environment (2008), doi:10.1016/j.atmosenv.2008.02.034

reported for the Indian subcontinent (4.4± 0.9 $m^2 g^{-1}$ for sub-1 μm and 3.5 ± 0.6 for sub-10 μm ranges) (Quinn et al., 2002), but comparable with α_{sp} of 7.5–8.2 $m^2 g^{-1}$ for PM_3 in Denver (Sloane et al., 1991). However, $\alpha_{sp,dry,nss-sulfate}$ at Xinken fall within the theoretical range of low RH sulfate scattering efficiencies, 3.6–7.5 $m^2 g^{-1}$, revisited by Charlson et al. (1999). α_{sp} of sub-1 μm and sub-10 μm POM are 6.7 ± 1.3 and 4.7 ± 1.1 $m^2 g^{-1}$, respectively. Those values lie within the range of $\alpha_{ep;sp,POM}$ in the previous studies (Groblicki et al., 1981; Sloane, 1986; Sloane et al., 1991; Baik et al., 1996; Quinn et al., 2001, 2002, 2004).

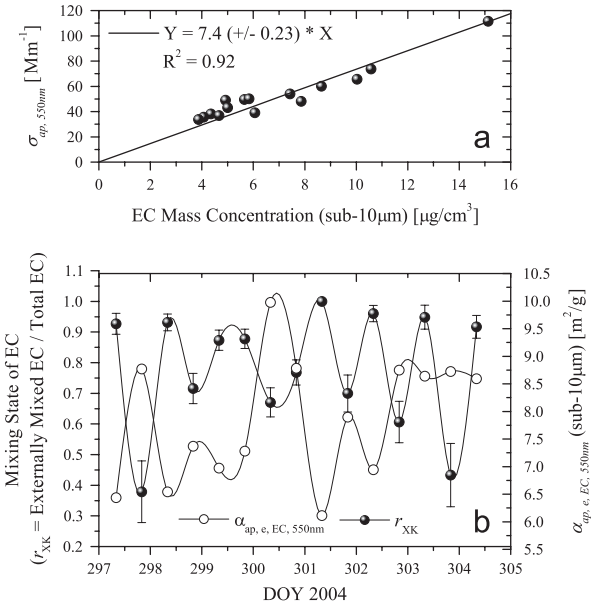

Fig. 12. (a) Linear correlation between the measured absorption coefficient at 550 nm ($\sigma_{ap,e,550\,nm}$) and sub-10 μm elemental carbon (EC) concentration from the impactor analysis, with slope and relative correlation coefficient (R^2). (b) Relationship between the calculated the attenuation cross section (the ratio of the measured $\sigma_{ap,e,550\,nm}$ and sub-10 μm EC concentration) and the EC mixing state (the mass ratio of the externally mixed EC and the total EC, and the error bar presents the uncertainties at 68% confidence level derived by a Monte Carlo simulation (Cheng et al., 2006)).

α_{sp} of residual in sub-1 μm particles is 5.7 ± 1.5 $m^2 g^{-1}$ at Xinken, which is higher than 3.0–3.4 $m^2 g^{-1}$ for Korea and Japan (Quinn et al., 2004). $\alpha_{sp,residual}$ in the sub-10 μm range is 1.5 ± 0.4 $m^2 g^{-1}$, which is within the range of 0.89–1.9 $m^2 g^{-1}$ for dust or residual in $PM_{2.5/10}$ reported in other open literature (Groblicki et al., 1981; Sloane, 1986; Baik et al., 1996; Quinn et al., 2004). α_{sp} of nitrate in sub-1 μm and sub-10 μm ranges are 7.6 ± 1.6 and 2.5 ± 1.2 $m^2 g^{-1}$, respectively. α_{sp} of nitrate was reported as 2.8 $m^2 g^{-1}$ in $PM_{2.5}$ by Groblicki et al. (1981) and as 3.37 $m^2 g^{-1}$ in PM_3 by Baik et al. (1996). $\alpha_{ep;sp}$ of sea salt, nitrate and residual for the sub-1 μm range are much higher than those for the sub-10 μm range. This may due to that the major masses of all those three chemical components are at super-1 μm range (Liu et al., 2008a).

The specific attenuation cross-section (α_{ap}) is also a factor used to convert the attenuation of a light beam due to the absorption of aerosols measured by filter-based measurements or other technique (e.g. photoacoustic) into the black carbon content. At Xinken, α_{ap} for sub-1 μm and sub-10 μm EC are 9.3 ± 1.4 and 7.2 ± 1.0 $m^2 g^{-1}$, respectively. As shown in Fig. 12a, from the linear regression of the measured $\sigma_{ap,550\,nm}$ against the analyzed EC concentrations from the impactor samples for sub-10 μm particles, $\alpha_{ap,EC,550\,nm}$ (sub-10 μm) is 7.4 ± 0.2 $m^2 g^{-1}$. It is comparable with the result from the Mie calculation. Moreover, $\alpha_{ap,EC}$ at Xinken falls into the estimated range of 5–20 $m^2 g^{-1}$ by Liousse et al. (1993). $f_{ap,dry}$ of

Table 3
Mass extinction, scattering and absorption efficiencies for sub-1 μm and sub-10 μm particles at 550 nm in units of $m^2 g^{-1}$

	Sea salt	Nitrate	Sulfate	POM	EC	Residual	Aerosol
Sub-1 μm							
α_{ep}	4.4±2.2	8.0±1.6	7.5±1.3	7.1±1.3	11.0±1.4	6.2±1.6	7.6±1.1
α_{sp}	4.1±2.1	7.6±1.6	7.1±1.4	6.7±1.3	4.2±0.8	5.7±1.5	6.4±1.1
α_{ap}	–	–	–	0.06±0.01	9.3±1.4	0.23±0.05	–
Sub-10 μm							
α_{ep}	1.5±1.0	2.6±1.2	6.1±1.1	4.9±1.1	8.5±1.3	1.7±0.5	4.1±0.8
α_{sp}	1.4±0.9	2.5±1.2	5.8±1.1	4.7±1.1	3.3±0.7	1.5±0.4	3.5±0.8
α_{ap}	–	–	–	0.05±0.01	7.2±1.0	0.12±0.03	–

Please cite this article as: Cheng, Y.F., et al., Aerosol optical properties and related chemical apportionment at Xinken in Pearl River Delta of China. Atmospheric Environment (2008), doi:10.1016/j.atmosenv.2008.02.034

POM and residual are less than 10%, and their α_{ap} are very small (0.06 and 0.23 $m^2 g^{-1}$ in sub-1 μm range, 0.05 and 0.12 $m^2 g^{-1}$ in sub-10 μm range, respectively), compared with the α_{ap} of POM (3.8 $m^2 g^{-1}$) from the multiple linear regression by (Groblicki et al., 1981).

Liousse et al. (1993) indicated that the $\alpha_{ap,EC}$ displayed an important variability which may relate to the variability of the aerosol mixing state and the aging of the atmospheric particles. From 297 to 304 DOY, the mixing state of EC at Xinken, defined as the mass ratio of externally mixed EC to the total EC (r_{XK}), has been estimated by an in situ dry optical closure study (Cheng et al., 2006). In light of the aforementioned fact that over 90% of σ_{ap} is contributed by EC, a time series of $\alpha_{ap,e,EC}$ are calculated as the ratio of measured $\sigma_{ap,e,550\,nm}$ and the EC mass concentration for sub-10 μm particles. Even though the variation of $\alpha_{ap,EC}$ is not only influenced by the mixing state of EC, but also effected by many other factors, such as air mass changing, different aerosol sources and atmospheric conditions, a fairly good anti-correlation between $\alpha_{ap,e,EC}$ (sub-10 μm) and r_{XK} can be found in Fig. 12b. It implies a higher $\alpha_{ap,EC}$ in the case of more internally mixed EC content under the atmospheric conditions of Xinken. Bond et al. (2006) indicate that the amplification of σ_{ap} due to the mixing of particulate materials is particle diameter size dependent. However, the absorption cross-section per absorbing mass increases by removing absorbing material and adding non-absorbing material without changing its size. In the present study, $D_{p,eff}$ are around 250–350 nm (Fig. 4). The volume fraction of EC is about 10–15% (Liu et al., 2008a). As shown in Fig. 3 of Bond et al. (2006), when D_p is around 250–300 nm and volume fraction of absorbing material is about 10–15%, the absorption cross-section per absorbing mass is estimated to be about 10–12 $m^2 g^{-1}$. When all of those EC (absorbing material) is externally mixed with other particle non-absorbing material, the diameter of EC may be about 80–100 nm. By checking the absorption cross-section at absorbing volume fraction of 1.0, it can be found that the absorption cross-section theoretically calculated by Bond et al. (2006) is about 6.0 $m^2 g^{-1}$. These results are consistent with our estimation. As one can see in Fig. 12b, when EC mixing state changing from external to internal mixture (EC mixing ratio from about 0.2 to 1.0), the $\alpha_{ap,EC}$ increases from around 6.0 to 10.0 $m^2 g^{-1}$.

4.4.2. Size distributions of the aerosol optical properties

The diversities in $\alpha_{ep;sp;ap,i}$ among different kinds of aerosol chemical compositions or sub-aerosol-populations are mainly due to the differences in their $\tilde{m}$ and size distributions (Lelieveld and Heintzenberg, 1992). To examine the size range of particle responsible for σ_{ep}, the aerosol light extinction size distributions are calculated for internal and external mixtures, as shown in Fig. 13. The importance of sub-micrometer mode particles to σ_{ep}, and in particular, those having Stokes diameter ($D_{p,Stokes}$) near the peak of the solar spectrum of about 500 nm (Seinfeld and Pandis, 1998) is apparent. This result is consistent with other studies (Bergin et al., 2001; Carrico et al., 2003). It is worthwhile to note that the sub-1 μm particles dominate the contribution to σ_{ep} with a factor of 93%, however, the super-1 μm particles only contribute about 7% at Xinken. Bergin et al. (2001) reported that f_{sp} that is due to sub-1 μm (aerodynamic diameter) particles ranged from 68% to 82% in Beijing of June 1999. During INDOEX 1999, the sub-1 μm to sub-10 μm extinction ratios are only about 28% for South Hemispheric Atlantic and 40% for South Hemispheric Indian Ocean, where sea salt dominates in the super-1 μm range. But the respective values for Indian subcontinent and East Indian subcontinent are as high as 92% and 89% (Quinn et al., 2002), which is comparable with our results.

The mean aerosol light scattering and absorption size distributions of different chemical components

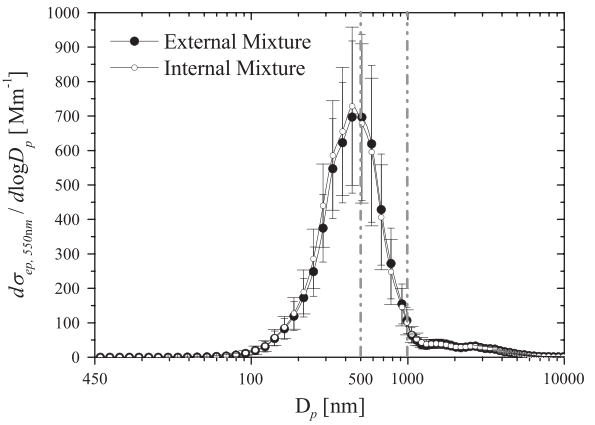

Fig. 13. Average aerosol extinction size distributions at 550 nm for external and internal mixtures. The error bars present one standard deviation during the whole period of 297–304 DOY 2004.

Please cite this article as: Cheng, Y.F., et al., Aerosol optical properties and related chemical apportionment at Xinken in Pearl River Delta of China. Atmospheric Environment (2008), doi:10.1016/j.atmosenv.2008.02.034

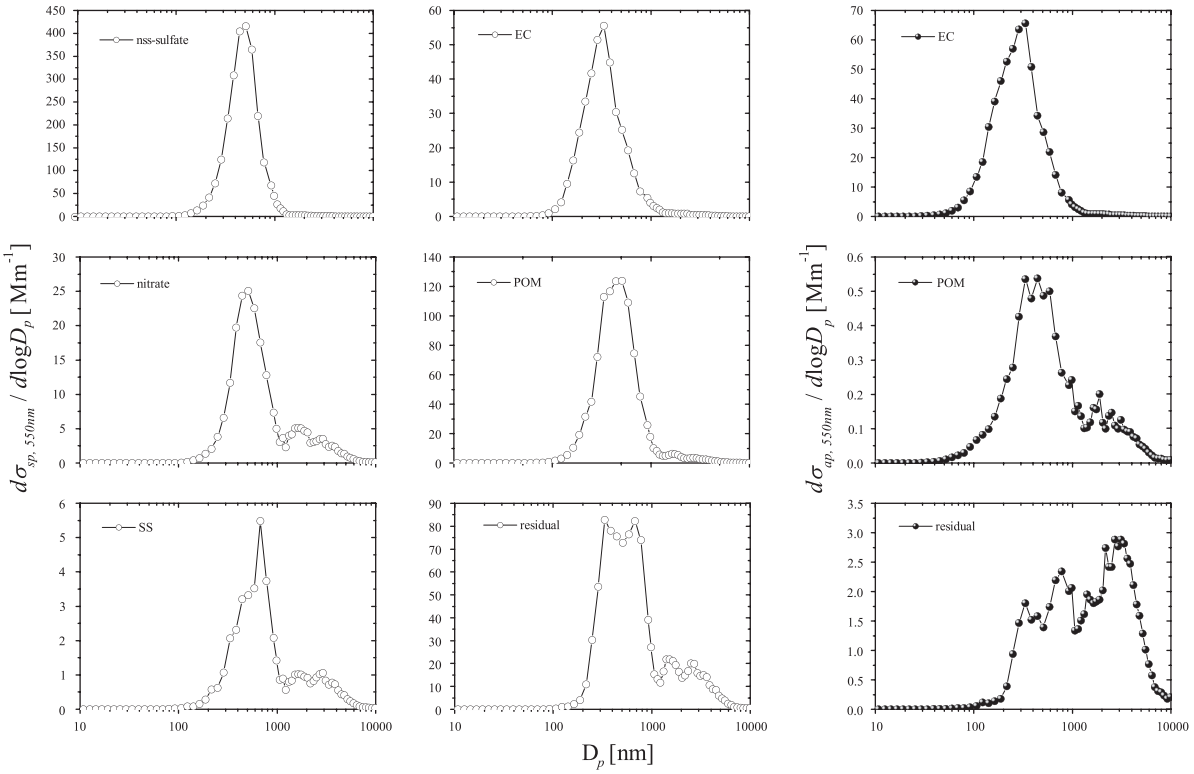

Fig. 14. Average aerosol scattering and absorption size distributions at 550 nm of individual aerosol chemical compositions during the whole period of 297–304 DOY 2004, calculated with external mixture. For the clarity of the figures, the standard deviations are not presented here.

are calculated with external mixture (Fig. 14). There is only one mode peaking at 500 nm in the scattering size distribution of nss-sulfate. The shape of EC scattering and absorption size distributions is similar with that of nss-sulfate, but the peaks both occur at smaller size of ~300 nm. The scattering size distributions of sea salt, nitrate, POM and residual all show three modes. The first peaks are at 600, 500, 500, 300–800 nm, respectively; the second peaks are at about 1400–1700 nm; and the third peaks are at about 3000 nm. However, the relative f_{sp} of sea salt, nitrate and residual in the super-1 μm range is greater than that of POM. It is obvious that the absorption size distributions of POM and residual are different from that of EC, though they only contribute about 10% to σ_{ap}. There is a broad mode peaking from 250 to 700 nm in the absorption size distribution of POM, and also a small contribution due to the POM in super-1 μm range. In the case of residual, more than half of the σ_{ap} is due to the super-1 μm residual.

5. Summary and conclusions

During the intensive field campaign from 4 October to 5 November 2004, the optical properties of sub-10 μm dry aerosol particles (RH < 20%) are investigated at Xinken in PRD of China. Compared with the open literature, severe aerosol optical pollution has been found at Xinken characterized by strongly light-absorbing particles. At 550 nm, the magnitude of the light scattering ($333 \pm 138\ \mathrm{Mm^{-1}}$) and absorption ($70 \pm 42\ \mathrm{Mm^{-1}}$), limited visual range (5.3 ± 2.5 km), and low single scattering albedo (0.83 ± 0.05) show Xinken to be comparable to the most polluted urban cores rather than even a polluted rural site. Other presented AOPs include hemispheric backscattering fraction ($11 \pm 1\%$) and asymmetry parameter (0.67 ± 0.01) at 550 nm, and Ångström exponent ($\mathring{a}_{450/700} = 1.6 \pm 0.15$).

Systematic relationships exist between various AOPs (σ_{sp}, σ_{ap}, ω_0, $\beta(1)$, and $\mathring{a}$), especially during N/NE and S/SE periods. It is also found that the diurnal variation in AOPs cannot be solely

Please cite this article as: Cheng, Y.F., et al., Aerosol optical properties and related chemical apportionment at Xinken in Pearl River Delta of China. Atmospheric Environment (2008), doi:10.1016/j.atmosenv.2008.02.034

explained by dilution as the PBL development during the day. It is also influenced by the local wind patterns, sources variation, photochemistry, and nighttime heterogeneous chemistry.

Based on the dry and ambient closure studies of the AOPs, $f_{ep;sp;ap,i}$ due to individual aerosol chemical compositions or sub-aerosol-populations (sub-1 μm and sub-10 μm) are calculated by Mie model with the size-segregated aerosol chemical compositions and number size distribution in an external mixture. The sub-1 μm particles contribute over 90% of $\sigma_{ep,550\,nm} \cdot f_{ep,dry,i,550\,nm}$ of nss-sulfate, POM, EC and residual are about 44%, 17%, 17% and 15%, respectively. The contributions to $\sigma_{ep,dry,550\,nm}$ due to SS and nitrate are less than 5%. However, at Xinken, the water taken up by the water soluble particle matters can contribute up to 50–60% of σ_{ep} at RH 90%. So in the ambient atmosphere, sulfate and carbonaceous (POM + EC), as well as the water, all play very important roles, concerning the visibility impairment at Xinken, especially during the day with high RH.

Consequently, $\alpha_{ep;sp,550\,nm}$ of sub-1 μm and sub-10 μm particles and individual chemical compositions can be derived. They are mostly consistent with previously reported values for the polluted area. α_{ep} of sub-1 μm and sub-10 μm particles are, respectively, 7.6 and 4.1 $m^2\,g^{-1}$. α_{sp} for sub-1 μm and sub-10 μm nss-sulfate are 7.1 and 4.7 $m^2\,g^{-1}$, respectively. The respective values for sub-1 μm and sub-10 μm POM are 6.7 and 4.7 $m^2\,g^{-1}$. α_{sp} of residual in sub-1 μm particles is 5.7 $m^2\,g^{-1}$ and in sub-10 μm range is only 1.5 $m^2\,g^{-1}$. α_{sp} of nitrate in sub-1 μm and sub-10 μm ranges are 7.6 and 2.5 $m^2\,g^{-1}$, respectively. α_{sp} of SS, nitrate and residual for sub-1 μm particles are much higher than those for sub-10 μm particles, which may due to that there are also considerable masses of all those three chemical components lie in the super-1 μm range.

At Xinken, $\alpha_{ap,550\,nm}$ of EC is 9.3 and 7.2 $m^2\,g^{-1}$, respectively, for the sub-1 μm and sub-10 μm ranges, with a contribution to σ_{ap} over 90%. Even though, the variation of $\alpha_{ap,EC}$ may be not only influenced by the mixing state of EC, a fairly good anti-correlation between the $\alpha_{ap,e,EC}$ of sub-10 μm EC and externally mixed EC mass ratio has been found. It implies a higher $\alpha_{ap,EC}$ in case more internal mixed EC content under the atmospheric conditions of Xinken. f_{ap} by POM and residual are less than 10%, and their α_{ap} are very small.

At last, the diversities in $\alpha_{ep;sp;ap,i}$ are investigated with the calculated scattering and absorption size distributions of different aerosol chemical compositions.

The in situ ground-based aerosol optical measurements in our study can be used to constrain the assumptions of the AOPs in column radiative forcing estimations. Chemical apportionment of the light extinction at Xinken provides a basis for implementing strategies to address and cope with the severe pollution problems in the PRD of China, a rapidly developing region.

Acknowledgments

This study was mainly supported by *China National Basic Research and Development Programs 2002CB410801 and 2002CB211605*. We also acknowledge *Gottlieb Daimler and Karl Benz Foundation* for the scholarship supporting the study of Y.F. Cheng in Leibniz-Institute for Tropospheric Research (I*f*T), Leipzig, Germany.

References

Ackerman, T.P., Toon, O.B., 1981. Absorption of visible radiation in atmosphere containing mixtures of absorbing and nonabsorbing particles. Applied Optics 20 (20), 3661–3668.

Anderson, T.L., Ogren, J.A., 1998. Determining aerosol radiative properties using the TSI 3563 Integrating Nephelometer. Aerosol Science and Technology 29, 57–69.

Anderson, T.L., Covert, D.S., Marshall, S.F., Laucks, M.L., Charlson, R.J., Waggoner, A.P., Ogren, J.A., Caldow, R., Holm, R.L., Quant, G., Sem, J., Wiedensohler, A., Ahlquist, N.A., Bates, T.S., 1996. Performance characteristics of a High-sensitivity, three-wavelength total scatter/backscatter nephelometer. Journal of Atmospheric and Oceanic Technology 13, 967–986.

Andreae, M.O., Gelencsèr, A., 2006. Black carbon or brown carbon? The nature of light-absorbing carbonaceous aerosols. Atmospheric Chemistry and Physics Discussions 6, 3419–3463.

Andreae, M.O., Schmid, O., Yang, H., Chand, D., Yu, J.Z., Zeng, L.-M., Zhang, Y.-H., 2008. Optical properties and chemical composition of the atmospheric aerosol in urban Guangzhou, China. Atmospheric Environment, this issue, doi:10.1016/j.atmosenv.2008.01.030.

Ångström, A., 1964. The parameters of atmospheric turbity. Tellus 16, 64–75.

Ansmann, A., Engelmann, R., Althausen, D., Wandinger, U., Hu, M., Zhang, Y., He, Q., 2005. High aerosol load over the Pearl River Delta, China, observed with Raman lidar and Sun photometer. Geophysical Research Letters 32 (L13815).

Baik, N.-J., Kim, Y.P., Moon, K.C., 1996. Visibility study in Seoul, 1993. Atmospheric Environment 30 (13), 2319–2328.

Bergin, M.H., Ogren, J.A., Schwartz, S.E., McInnes, L.M., 1997. Evaporation of ammonium nitrate aerosol in a heated nephelometer: implications for field measurements. Environmental Science and Technology 31, 2878–2883.

Bergin, M.H., Gass, G.R., Xu, J., Fang, C., Zeng, L.M., Yu, T., Salmon, L.G., Kiang, C.S., Tang, X.Y., Zhang, Y.H., Chameides, W.L., 2001. Aerosol radiative, physical, and chemical properties in Beijing during June 1999. Journal of Geophysical Research 106 (D16), 17,969–17,980.

Birmili, W., Stratmann, F., Wiedensohler, A., 1999. Design of a DMA-based size spectrometer for a large particle size range and stable operation. Journal of Aerosol Science 30 (4), 549–553.

Birmili, W., Nowak, A., Schwirn, K., Lehmann, K., Massling, A., Wiedensohler, A., 2004. A new method to accurately relate dry and humified number size distributions of atmospheric aerosols. Journal of Aerosol Science 1, 15–16 (abstracts of European Aerosol Conference).

Bodhaine, B.A., 1995. Aerosol absorption measurements at Barrow, Mauna Loa and the south pole. Journal of Geophysical Research 100 (D5), 8967–8975.

Bohren, C.F., Huffman, D.R., 1998. Absorption and Scattering of Light by Small Particles. Wiley, Inc., New York.

Bond, T.C., Bergstrom, R.W., 2006. Light absorption by carbonaceous particles: an investigative review. Aerosol Science and Technology 40, 27–67.

Bond, T.C., Charlson, R.J., Heintzenberg, J., 1998. Quantifying the emission of light-absorption particles: measurements tailored to climate studies. Geophysical Research Letters 25 (3), 337–340.

Bond, T.C., Habib, G., Bergstrom, R.W., 2006. Limitations in the enhancement of visible light absorption due to mixing state. Journal of Geophysical Research 111, D20211.

Bucholtz, A., 1995. Rayleigh-scattering calculations for the terrestrial atmosphere. Applied Optics 34 (15), 2765–2773.

Carrico, C.M., Rood, M.J., Ogren, J.A., 1998. Aerosol light scattering properties at Cape Grim, Tasmania, during the First Aerosol Characterization Experiment (ACE 1). Journal of Geophysical Research 103 (D13), 16,565–16,574.

Carrico, C.M., Rood, M.J., Ogren, J.A., Neusüss, C., Wiedensohler, A., Heinzenberg, J., 2000. Aerosol optical properties at Sagres Portugal, during ACE-2. Tellus 52B, 694–715.

Carrico, C.M., Bergin, M.H., Xu, J., Baumann, K., Maring, H., 2003. Urban aerosol radiative properties: measurements during the 1999 Atlanta Supersite Experiment. Journal of Geophysical Research 108 (D7), 8422.

Charlson, R.J., Anderson, T.L., Rodhe, H., 1999. Direct climate forcing by anthropogenic aerosols: quantifying the link between atmospheric sulfate and radiation. Contributions to Atmospheric Physics 72 (1), 79–94.

Charlson, R.J., Schwartz, S.E., Hales, J.M., Cess Jr., J.A.C., Hansen, J.E., Hofmann, D.J., 1992. Climate forcing by anthropogenic aerosols. Science 255, 423–430.

Cheng, Y.F., Eichler, H., Wiedensohler, A., Heintzenberg, J., Zhang, Y.H., Hu, M., Herrmann, H., Zeng, L.M., Liu, S., Gnauk, T., Brüggemann, E., He, L.Y., 2006. Mixing state of elemental carbon and non-light-absorbing aerosol components derived from in situ particle optical properties at Xinken in Pearl River Delta of China. Journal of Geophysical Research 111, D20204.

Cheng, Y.F., Wiedensolher, A., Eichler, H., Heintzenberg, J., Tesche, M., Ansmann, A., Wendisch, M., Su, H., Althause, D., Herrmann, H., Gnauk, T., Brüggemann, E., Hu, M., Zhang, Y.H., 2008. Relative humidity dependence of aerosol optical properties and direct radiative forcing in the surface boundary layer of South-Eastern China: an observation based numerical study. Atmospheric Environment, submitted for publication.

Chýlek, P., Wong, J., 1995. Effect of absorbing aerosols on global radiation budget. Geophysical Research Letters 22 (8), 929–931.

Clarke, A., McNaughton, C., Kapustin, V., Shinozuka, Y., Howell, S., Dibb, J., Zhou, J., Anderson, B., Brekhovskikh, V., Turner, H., Pinkerton, M., 2007. Biomass burning and pollution aerosol over North America: organic components and their influences on spectral optical properties and humidification response. Journal of Geophysical Research 112 (D12S18).

Coen, M.C., Weingartner, E., Schaub, D., Hueglin, C., Corrigan, C., Henning, S., Schwikowski, M., Baltensperger, U., 2004. Saharan dust events at the Jungfraujoch: Detection by wavelength dependence of the single scattering albedo and first climatology analysis. Atmospheric Chemistry and Physics 4, 2465–2480.

Covert, D.S., Charlson, R.J., Ahlquist, N.C., 1972. A study of the relationship of chemical composition and humidity to light scattering by aerosols. Journal of Applied Meterology 11, 968–976.

Covert, D.S., Heintzenberg, J., Hansson, H.C., 1990. Electro-optical detection of external mixtures in aerosols. Aerosol Science and Technology 12, 446–456.

d' Almeida, G., Keopke, P., Shettle, E., 1991. Atmospheric Aerosols—Global Climatology and Radiative Characteristics. A. Deepak, Hampton, VA.

Delene, D.J., Ogren, J.A., 2002. Variability of aerosol optical properties at four North America surface monitoring sites. Journal of Atmospheric Science 59 (6), 1135–1150.

Egan, W.G., Hilgeman, T., 1980. Anomalous refractive index of submicron-sized particles. Applied Optics 19, 3724–3727.

Eichler, H., Cheng, Y.F., Birmili, W., Wiedensohler, A., Brüggemann, E., Gnauk, T., Herrmann, H., Althausen, D., Ansmann, A., Engelmann, R., Tesche, M., Zhang, Y.H., Hu, M., Liu, S., Zeng, L.M., 2008. Hygroscopic properties and ambient extinction of aerosol particles in South-Eastern China. Atmospheric Environment, submitted for publication.

Eldering, A., Ogren, J.A., Chowdhury, Z., Hughes, L.S., Gass, G.R., 2002. Aerosol optical properties during INDOEX based on measured aerosol particle size and composition. Journal of Geophysical Research 107 (D22), 8001.

Fröhlich, C., Shaw, G.E., 1980. New determination of Rayleigh scattering in the terrestrial atmosphere. Applied Optics 19 (11), 1773–1775.

Griffing, G.W., 1980. Relations between the prevailing visibility, nephelometer scattering coefficient and sunphotometer turbidity coefficient. Atmospheric Environment 14, 577–584.

Groblicki, P.J., Wolff, G.T., Countess, R.J., 1981. Visibility-reduction species in the Denver "Brown Cloud"—I. Rlaitionships between extinction and chemical composition. Atmospheric Environment 12, 2437–2484.

Hänel, G., 1987. Radiation budget of the boundary layer: part II. Simultaneous measurement of mean solar volume absorption and extinction coefficients of particles. Contributions to Atmospheric Physics 60, 241–247.

Please cite this article as: Cheng, Y.F., et al., Aerosol optical properties and related chemical apportionment at Xinken in Pearl River Delta of China. Atmospheric Environment (2008), doi:10.1016/j.atmosenv.2008.02.034

Hasan, H., Dzubay, T.G., 1983. Apportioning light extinction coefficients to chemical species in atmospheric aerosol. Atmospheric Environment 17, 1573–1581.

Heintzenberg, J., Charlson, R.J., 1996. Design and applications of the integrating nephelometer: a review. Journal of Atmospheric and Oceanic Technology 13, 987–1000.

Heintzenberg, J., Cheng, Y.F., Wehner, B., 2008. Long-term measurements of aerosol size distribution and visibility in Beijing during 2004 – 2007, in preparation.

HOCP, 1963. Handbook of Chemistry and Physics. The Chemical Rubber Publishing Co., Cleveland, OH.

Hoffer, A., Gelncs'er, A., Guyon, P., Kiss, G., Schmid, O., Frank, G.P., Artaxo, P., Andreae, M.O., 2006. Optical properties of humic-like substances (HULIS) in biomass-burning aerosols. Atmospheric Chemistry and Physics 6, 3563–3570.

Holland, H.D., 1978. The Chemistry of the Atmospheric and Oceans. Wiley, New York, p. 154.

Hu, M., Wu, Z., Slanina, J., Lin, P., Liu, S., Zeng, L., 2008. Acidic gases, ammonia and water-soluble ions in $PM_{2.5}$ at a coastal site in the Pearl River Delta, China. Atmospheric Environment, this issue, doi:10.1016/j.atmosenv.2008.02.015.

Huebert, B.J., Bates, T., Russell, P.B., Shi, G., Kim, Y.J., Kawamura, K., Carmichael, G., Nakajima, T., 2003. An overview of ACE-Asia: strategies for quantifying the relationships between Asian aerosols and their climatic impacts. Journal of Geophysical Research 108 (D23), 8633 ⟨http://www.agu.org/journals/jd/jd0321/2003JD003550/⟩.

Husar, R.B., Husar, J.D., Martin, L., 2000. Distribution of continental surface aerosol extinction based on visual range data. Atmospheric Environment 34, 5067–5078.

IPCC, 2007. Climate change 2007: the physical science basis. Contribution of Working Group I to the Fourth Assessment Report of the Intergovernmental Panel on Climate Change. Cambridge University Press, Cambridge, UK and New York, NY, USA.

Jacobson, M.Z., 2001. Strong radiative heating due to the mixing state of black carbon in atmospheric aerosol. Nature 409, 695–697.

Kent, G., Yue, G.K., Farrukh, U.O., Deepak, A., 1983. Modeling atmospheric aerosol backscatter at CO_2 laser wavelengths, 1. Aerosol properties modeling techniques and associated problems. Applied Optics 22, 1655–1665.

Kim, S.-W., Yoon, S.-C., Jefferson, A., Ogren, J.A., Dutton, E.G., Won, J.-G., Ghim, Y.S., Lee, B.-I., Han, J.-S., 2005. Aerosol optical, chemical and physical properties at Gosan, Korea during Asian dust and pollution episodes in 2001. Atmospheric Environment 39, 39–50.

Koloutsou-Vakakis, S., Carrico, C.M., Kus, P., Rood, M.J., Li, Z., Shrestha, R., Ogren, J.A., Chow, J.C., Watson, J.G., 2001. Aerosol properties at a midlatitude Northern Hemisphere continental site. Journal of Geophysical Research 106 (D3), 3019–3032.

Lelieveld, J., Heintzenberg, J., 1992. Sulfate cooling effect on climate through in-cloud oxidation of anthropogenic SO_2. Science 258, 117–120.

Lesins, G., Chylek, P., Lohman, U., 2002. A study of internal and external mixing scenarios and its effect on aerosol optical properties and direct radiative forcing. Journal of Geophysical Research 107 (D10), 4094.

Liousse, C., Cachier, H., Jennings, S.G., 1993. Optical and thermal measurements of black carbon aerosol content in different environments: variation of the specific attenuation cross-section, sigma (σ). Atmospheric Environment 27A (8), 1203–1211.

Liu, S., Hu, M., Slanina, S., He, L.-Y., Niu, Y.-W., Brüggemann, E., Gnauk, T., Herrmann, H., 2008a. Size distribution and source analysis of ionic compositions of aerosols in polluted periods at Xinken in Pearl River Delta (PRD) of China. Atmospheric Environment, this issue, doi:10.1016/j.atmosenv.2007.12.035.

Liu, S., Hu, M., Wehner, B., Wiedensohler, A., Cheng, Y., 2008b. Aerosol number size distribution and new particle formation at a rural/coastal site in Pearl River Delta PRD of China. Atmospheric Environment, in this issue, doi:10.1016/j.atmosenv.2008.01.063.

Louie, P.K.K., Waston, J.G., Chow, J.C., Chen, A., Sin, D.W.M., Lau, A.K.H., 2005. Seasonal characteristics and regional transport of $PM_{2.5}$ in Hong Kong. Atmospheric Environment 39, 1695–1710.

Mallet, M., Roger, J.C., Despiau, S., Dubovik, O., Putaud, J.P., 2003. Microphysical and optical properties of aerosol particles in urban zone during ESCOMPTE. Atmospheric Research 69, 73–79.

Malm, W.C., Sisler, J.F., Huffman, D., Eldred, R.A., Gahill, T.A., 1994. Spatial and seasonal trends in particle concentration and optical extinction in the United Sates. Journal of Geophysical Research 99 (D1), 1347–1370.

Man, C.K., Shih, M.Y., 2001. Light scattering and absorption properties of aerosol particles in Hong Kong. Journal of Aerosol Science 32, 795–804.

McGraw-Hill, 1928. International critical tables. Technical Report.

Nessler, R., Weingartner, E., Baltensperger, U., 2005. Effect of humidity on aerosol light absorption and its implications for extinction and the single scattering albedo illustrated for a site in the lower free troposphere. Journal of Aerosol Science 36 (8), 958–972.

Ogren, J.A., 1995. A systematic approach to in-situ observations of aerosol properties. In: Heitzenberg, J., Charlson, R.J. (Eds.), Aerosol Forcing of Climate. Wiley, New York, pp. 215–226.

Ouimette, J.R., Flagan, R.C., 1982. The extinction coefficient of multicomponent aerosols. Atmospheric Environment 16, 2405–2419.

Pesava, P., Horvath, H., Kasahara, M., 2001. A local optical closure experiment in Vienna. Journal of Aerosol Science 32, 1249–1267.

Petzold, A., Schönlinner, M., 2004. Multi-angle absorption photometrya new method for the measurement of aerosol light absorption and atmospheric black carbon. Journal of Aerosol Science 35, 421–441.

Quinn, P.K., Coffmann, D.J., 1998. Local closure during the first aerosol characterization experiment (ACE 1): aerosol mass concentration and scattering and backscattering coefficients. Journal of Geophysical Research 103 (D13), 16,575–16,596.

Quinn, P.K., Marshall, S.F., Bates, T.S., Covert, D.S., Kapustin, V.N., 1995. Comparison of measured and calculated aerosol properties relevant to the direct radiative forcing of tropospheric sulfate aerosol on climate. Journal of Geophysical Research 100 (D5), 8977–8991.

Quinn, P.K., Bates, T.S., Coffmann, D.J., Miller, T.L., Johnson, J.E., Covert, D.S., Putaud, J.-P., Neusüss, C., Novakov, T., 2000. A comparison of aerosol chemical and optical

properties from the 1st and 2nd aerosol characterization experiments. Tellus 52B, 239–257.

Quinn, P.K., Coffmann, D.J., Bates, T.S., Miller, T.L., Johnson, J.E., Voss, K., Welton, E.J., Neusüss, C., 2001. Dominant aerosol chemical components and their contribution to extinction during the Aerosols99 cruise across the Atlantic. Journal of Geophysical Research 106 (D18), 20,783–20,809.

Quinn, P.K., Coffman, D.J., Bates, T.S., Miller, T.L., Johnson, J.E., Welton, E.J., Neusüss, C., Miller, M., Sheridan, P.J., 2002. Aerosol optical properties during INDOEX 1999: means, variability, and controlling factor. Journal of Geophysical Research 107 (D19), 8020, doi:2000JD000037.

Quinn, P.K., Coffman, D.J., Bates, T.S., Welton, E.J., Covert, D.S., Miller, T.L., Johnson, J.E., Maria, S., Russell, L., Arimoto, R., Carrico, C.M., Rood, M.J., Anderson, J., 2004. Aerosol optical properties measured on board the Ronald H. Brown during ACE-Asia as a function of aerosol chemical composition and source region. Journal of Geophysical Research 109 (D19S01).

Redemann, J., Turco, R.P., Liou, K.N., Russell, P.B., Bergstrom, R.W., Schmid, B., Livingston, J.M., Hobbs, P.V., Hartley, W.S., Ismail, S., Ferrare, R.A., Browell, E.V., 2000. Retrieving the vertical structure of the effective aerosol complex index of refraction from a combination of aerosol in situ and remote sensing measurements during TARFOX. Journal of Geophysical Research 105 (D8), 9949–9970.

Reid, J.S., Hobbs, P.V., Ferek, R.J., Blake, D.R., Martins, J.V., Dunlap, M.R., Liousse, C., 1998. Physical chemical and optical properties of regional hazes dominated by smoke in Brazil. Journal of Geophysical Research 103 (D24), 32,059–32,080.

Remer, L.A., Kaufman, Y.J., 1998. Dynamic aerosol mode: urban/industrial aerosol. Journal of Geophysical Research 103 (D12), 13859–13871.

Schichtel, B.A., Husar, R.B., Falke, S.R., Wilson, W.E., 2001. Haze trends over the United States 1980–1995. Atmospheric Environment 35, 5205–5210.

Schkolnik, G., Chand, D., Hoffer, A., Andreae, M.O., Erlick, C., Swietlicki, E., Rudich, Y., 2007. Constraining the density and complex refractive index of elemental and organic carbon in biomass burning aerosol using optical and chemical measurements. Atmospheric Environment 41, 1107–1118.

Seinfeld, J., Pandis, S., 1998. Atmospheric chemistry and physics: from air pollution to climate change. Wiley, Inc., New York.

Sheridan, P.J., Delene, D.J., Ogren, J.A., 2001. Four years of continuous surface aerosol measurements from the Department of Energy's Atmospheric Radiation Measurement Program Southern Great Plains Could and Radiation Testbed site. Journal of Geophysical Research 106 (D18), 20735–20747.

Slanina, J., Brink, H.M.t., Otjes, R.P., Even, A., Jongejan, P., Khlystov, A., Waijers-Ijpelaan, A., Hu, M., Lu, Y., 2001. The continuous analysis of nitrate and ammonium in aerosols by the steam jet aerosol collector (SJAC): extension and validation of the methodology. Atmospheric Environment 35, 2319–2330.

Sloane, C.S., 1986. Effect of composition on aerosol light scattering efficiencies. Atmospheric Environment 20 (5), 1025–1037.

Sloane, C.S., Watson, J., Chow, J., Pritchett, L., Richards, L.W., 1991. Size-segregated fine particle measurements by chemical species and their impact on visibility impairment in Denver. Atmospheric Environment 25A, 1013–1024.

Su, H., Cheng, Y.F., Shao, M., Gao, D.F., Yu, Z.Y., Zeng, L.M., Slanina, J., Zhang, Y.H., Wiedensohler, A., 2008. OH formation by HONO photolysis and photolytic HONO sources during the Peal River Delta experiment in China 2004. Geophysical Research Letters, submitted for publication.

Tang, I.N., 1996. Chemical and size effects of hygroscopic aerosols on light scatterring coefficients. Journal of Geophysical Research 101 (D14), 19,245–19,250.

Tang, I.N., Munkelwitz, H.R., 1993. Composition and temperature dependence of the deliquescence properties of hygroscopic aerosols. Atmospheric Environment 27A (4), 467–473.

Tang, I.N., Munkelwitz, H.R., 1994. Water activities, densities and refractive indices of aqueous sulfates and sodium nitrate droplets of atmospheric importance. Journal of Geophysical Research 99, 18801–18808.

Tomasi, C., Vitale, V., Petkov, B., Lupi, A., Cacciari, A., 2005. Improved algorithm for calculations of Rayleigh-scattering optical depth in standard atmospheres. Applied Optics 44 (16), 3320–3341.

Turpin, B.J., Lim, H.-J., 2001. Species contributions to $PM_{2.5}$ mass concentrations: revisiting common assumptions for estimating organic mass. Aerosol Science and Technology 35, 602–610.

Waggoner, A.P., Weiss, R.E., 1980. Comparison of fine particle mass concentration and light scattering extinction in ambient aerosols. Atmospheric Environment 14, 623–626.

Wex, H., 2002. Closure and sensitivity studies on physical parameters of rural continental aerosols. Ph.D. Thesis, Leipzig University.

White, W.H., 1990. Contributions to light-extinction visibility: existing and historical conditions—causes and effects. Report 24, National Acid Precipitation Assessment Program, Washington, DC, available as NT1585-102 from National Technical Information Service, Springfield, VA.

Wu, D., Tie, X., Li, C., Ying, Z., Lau, A.K.-H., Huang, J., Deng, X., Bi, X., 2005. An extremely low visibility event over the Guangzhou region: a case study. Atmospheric Environment 39, 6568–6577.

Zhang, Y.H., Zhu, X.L., Slanina, S., Shao, M., Zeng, L.M., Hu, M., Bergin, M., Salmon, L., 2004. Aerosol pollution in some Chinese cities. Pure Applied Chemistry 76 (6), 1227–1239.

Please cite this article as: Cheng, Y.F., et al., Aerosol optical properties and related chemical apportionment at Xinken in Pearl River Delta of China. Atmospheric Environment (2008), doi:10.1016/j.atmosenv.2008.02.034